



Review article

Overview of structural, electronic, elastic, thermal, optical, and nuclear properties of Zr_2AC (A= Al, Si, P, S, Ge, As, Se In, Sn, Tl, and Pb) MAX phases: A brief review

Dumooa R. Hussein^{*}, Khalid K. Abbas^{**}, Ahmed M.H. Abdulkadhim Al-Ghaban

Department of Materials Engineering, University of Technology, P.O. Box 19006, Baghdad, Iraq

ARTICLE INFO

Keywords:

MAX phase
 Zr_2AC applications
 Ceramic
 Zr_2AC properties
 Structural properties

ABSTRACT

The Zr_2AC MAX phases are a family of ternary carbides ceramics that possess layered structures and exhibiting exceptional properties resulting from combining the most desirable features of metals and ceramics. In addition, the Zr_2AC MAX-phases exhibit numerous physical and chemical properties due to their chemical and structural characteristics, a tendency for multiple basal dislocations and exhibiting mobility under ambient conditions. This review extensively analyzes the properties of the Zr_2AC MAX phase, as they are closely linked to the exceptional and potential applications of the MAX phase. For the first time, the present study analyzed various properties of Zr_2AC MAX phases, including structural, electronic, elastic, thermal, optical, self-healing, nuclear, oxidation, and corrosion characteristics. Furthermore, this review included experimental and theoretical work with comparison. It's found that the Zr_2AC lattice parameters a and c are deviations theoretically from 0.1 to 2% and 0.15–2.87% compared with experimental work. Also, the Zr_2AC MAX phases are metallic characters and the conductivity differs depending on the type of the Zr_2AC (different A element) MAX phases. Its concluded that the Zr_2AC MAX phases are stiff, isotropic elastic properties and high machinability with damage tolerance and hardness levels ranging from 3.5 to 13.02 Gpa. The Zr_2AC MAX phases are also resistant to corrosion, thermal shock, and oxidation as well as lightweight. In addition, at elevated temperatures the transition from brittle to plastic behavior can be occurred in the Zr_2AC MAX phase. The Zr_2AC MAX phase's optical properties are anisotropic such as electrical conductivity and mechanical properties. This review study provides a comprehensive details assisting researches to deal with Zr_2AC MAX phase potentially for different applications.

1. Introduction

From over 80 ternary carbides, nitrides, and borides can produce the nanolaminate $M_{n+1}AX_n$ or MAX phases successfully. The symbol "M" denotes the early and late transitional metals belonging to a group 3–6 of the periodic table of elements, while Groups 12–16 are represented by A. The nitrogen, carbon, or boron are represented by X, and n is 1–3, with the highest experimental value being 6. The $M_{n+1}AX_n$ ceramic layers are sandwiched-like between one-atom-thick metallic A-layers. Fig. 1(d) illustrates the X component z [1–5].

^{*} Corresponding author.

^{**} Corresponding author.

E-mail addresses: Dumooa87@gmail.com, mae.19.05@grad.uotechnology.edu.iq (D.R. Hussein), Khalid.K.Abbas@uotechnology.edu.iq (K.K. Abbas).

<https://doi.org/10.1016/j.heliyon.2023.e18303>

Received 29 May 2023; Received in revised form 12 July 2023; Accepted 13 July 2023

Available online 28 July 2023

2405-8440/© 2023 The Author(s). Published by Elsevier Ltd. This is an open access article under the CC BY-NC-ND license (<http://creativecommons.org/licenses/by-nc-nd/4.0/>).

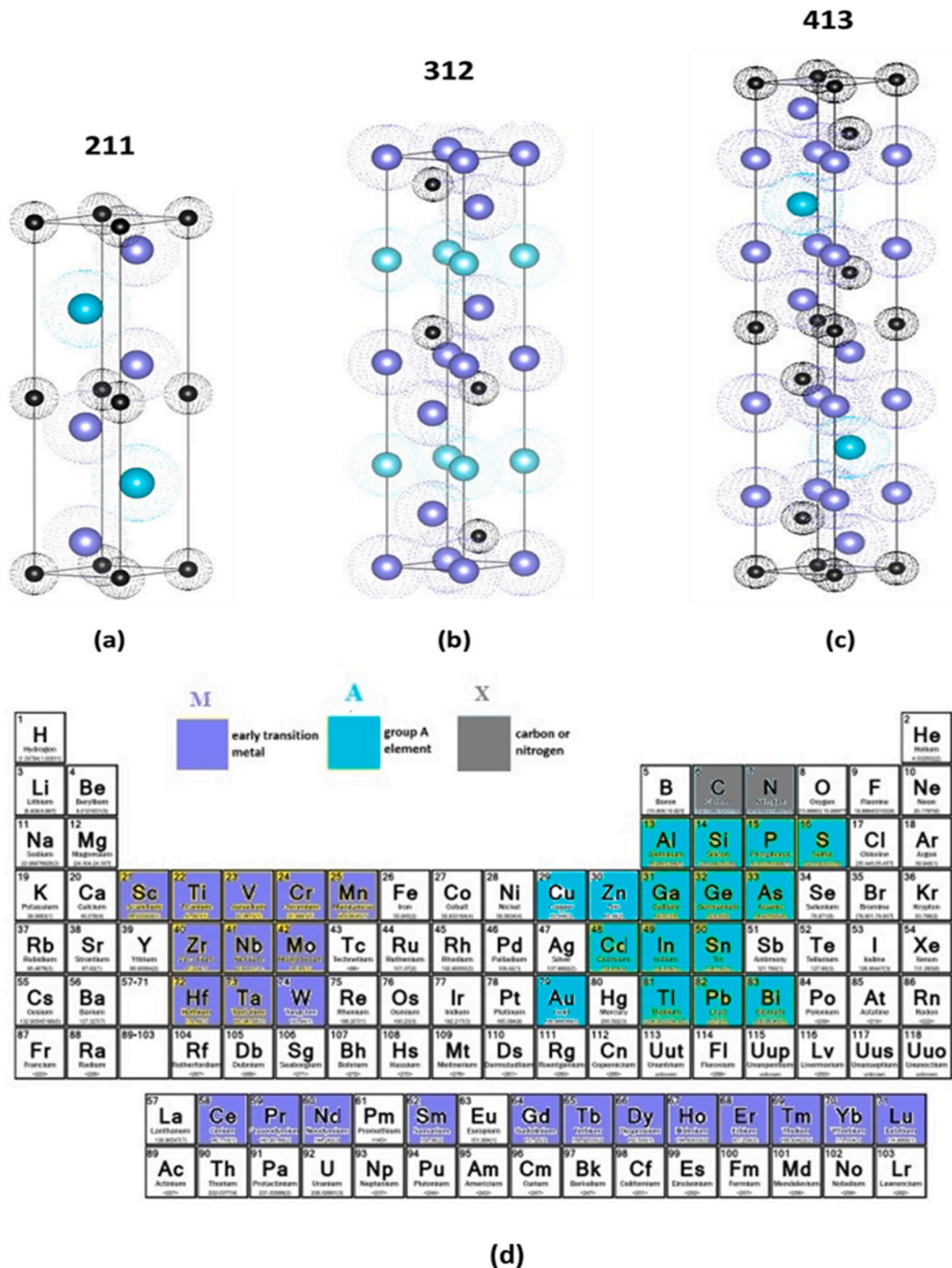


Fig. 1. The structures of crystal of MAX phase (a) 211, (b) 312, (c) 413 and (d) Periodic Table of Elements Displaying MAX Phases.

*(a–c) Drawing using the Materials Project website, Database version 2020_09_08. Powered by Pymatgen version 2022.0.8, combined with the VESTA program (Visualization for Electronic and Structural Analysis ver. 3.5.7, build data: Jan 7, 2021, copyright (c) 2006–2020 by Koichi Momma and Fuguo -Izumi). In addition to the periodic table, Fig. 1 (d) was created by using 2023 Science Notes and Projects, Designed by Press Customizer.

The term " $M_{n+1}AX_n$ " was recently reduced to "MAX". The M (transition metals) layers are close-packed in MAX phases. M layered is separated by A layers and filled with X atoms in octahedral locations [6]. This edge-sharing M_6X octahedral matches rock salt. Also, the MAX phases exhibit a classification system depending on their respective to "n" values: M_2AX (211 phase) [7], M_3AX_2 (312 phase) [8], M_4AX_3 (413 phase) [9], M_5AX_4 (514 phase) [10]. Additionally, the hybrid MAX phases include the 523 phase (composed of the 211 phase and the 312 phase) and the 725 phase is consisting of 413 and 314 phases) [11], M_2AB_2 (212 phase) and M_3AB_4 (314 phase)

boride MAX phases [12–14]. Moreover, there is another class of MAX phase, such as the 221 phase [15]. Fig. 1(a-b) shows that the three structures obtain different M-layers numbers between A layers and the periodic table displaying MAX phases. As a result, 211, 312, and 413 phases containing two, three, and four types, respectively. By similarity, the rest of the 514 phase, 615 phase, and 716 phase can be deduced from their structures.

This layer structure results in outstanding MAX phase characteristics [15]. The MAX phase is slightly soft, has great strength at high temperatures, and can be machined with no lubricating oil using standard high-speed tools [16]. The MAX phases are similar to metals in that had excellent thermal plus electrical conductivity with a good ability to machine, whereas the MAX phase has an electrical conductivity of $(12\text{--}60) \text{ W K}^{-1} \text{ m}^{-1}$ at ambient temperature. Due to the Fermi level, MAX phase metallic-like conductors have a high density of states indication for M elements by the d - d with $(0.07\text{--}2) \mu\Omega\cdot\text{m}$ resistivity. In some situations, their conductivities exceed their pure metal counterpart (M). The MAX phases exhibit exceptional optical characteristics. The MAX phase has thermal shock and oxidation resistance similar to ceramic [17–20]. Researchers demonstrated unusual thermal-shock behavior when the material's post-quenched strengths are higher than their pristine counterparts [20]. Ripplcation nucleation causes the MAX phases to deform when compressed, which leads to kink band behaviour. Additionally, the MAX phases are highly resistant to deterioration, obtaining 1.4 GPa to 8 GPa Vickers hardness and excellent plasticity at elevated temperatures.

MAX phases have shown excellent efficacy in an enormous variety of technical as well as industrial uses as the following:

1. Machinable refractories.
2. High-temperature component.
3. Electrical coatings
4. Nuclear requirement
5. Superconductivity component.
6. Fuel cells component.
7. Spintronics.
8. Thermal barrier coatings (TBC) [21].
9. Microscale mechanical pumping is used in various engineering fields [22].

In 2021, a study was conducted on incorporating cobalt and other metal dopants into ceramic materials [23]; the MAX phase can be used as high-performance ceramic materials.

Researchers have currently identified approximately 50 type of M_2AX phases. However, obtaining the possible combinations from MAX phases is thermodynamically unstable. Furthermore, substitutions on the "A," "M," with or without the "X" position, can produce an almost endless number of viable solutions [24–27]. Table 1 shows a collection of 211 available MAX phases (ternary) that were synthesized recently.

This review focuses on the main characteristics of the Zr_2AC MAX phase (211phase), where A element is Al, As, Tl, Pb, Sn, Si, S, P, In, or Ge. This review specifically discusses various characteristics of these nanolaminates, including the mechanical, optical, thermal, electronic, nuclear, and structural characteristics for the first time, which are relevant to their potential applications. More detailed information on these properties can obtain in the existing review. In addition, tables (2, 6, 9) summarize these properties to compare the mentioned types above of MAX phase or between the theoretical work with experiment work. This review concentrates on the main

Table 1

The collection of 211 available MAX Phases (ternary) [20].

Al	P	S	Ga	Ge
Ti ₂ AlC	V ₂ PC	Ti ₂ SC	Ti ₂ GaC	Ti ₂ GeC
V ₂ AlC	Nb ₂ PC	Zr ₂ SC	V ₂ GaC	V ₂ GeC
Cr ₂ AlC		Nb ₂ SC _{0.4}	Cr ₂ GaC	Cr ₂ GeC
Nb ₂ AlC		Nb ₂ SC	Nb ₂ GaC	Nb ₂ GeC
Ta ₂ AlC		Hf ₂ SC	Mo ₂ GaC	
Ti ₂ AlN			Ta ₂ GaC	
Zr ₂ AlC			Mn ₂ GaC	
Hf ₂ AlC			Ti ₂ GaN	
			Cr ₂ GaN	
			V ₂ GaN	
As	Zn	In	Sn	Tl
V ₂ AsC	Ti ₂ ZnC	Sc ₂ InC	Ti ₂ SnC	Ti ₂ TlC
Nb ₂ AsC	Ti ₂ ZnN	Ti ₂ InC	Hf ₂ SnN	Zr ₂ TlC
	V ₂ ZnC	Zr ₂ InC	Zr ₂ SnC	Hf ₂ TlC
		Nb ₂ InC	Nb ₂ SnC	Zr ₂ TlN
		Hf ₂ InC	Hf ₂ SnC	
		Ti ₂ InN	Lu ₂ SnC	
		Zr ₂ InN		
Pb	Precious metals		Others	
Ti ₂ PbC	Mo ₂ AuC		Ti ₂ CdC	
Zr ₂ PbC				
Hf ₂ PbC				

characteristics of the zirconium-based MAX phase (Zr_2AC), which is essential in advanced engineering applications such as nuclear, thermal barrier coating, solar heating, and high-temperature oxidation resistance parts.

The review aims to thoroughly understand Zr_2AC MAX phases, focusing on their recent progressive expansion and advancement.

2. Zr_2AC MAX phases

Fig. 2 displays crystals of MAX phases with a 211 (M_2AX) configuration, where zirconium, A, and carbon occupy Wyckoff positions of 4f, 2d, and 2a, respectively, as well as containing hexagonal structure as in the $P6_3/mmc$ space group [28].

The industrialization of nuclear reactors has been interesting in the Zr-MAX due to the atoms of Zirconium containing a tiny cross-sectional area as in thermal neutrons. Mechanical and thermal stresses are commonly observed in fuel cladding materials under intense conditions of the neutrons irradiation as well as intense oxidation or corrosion surrounding. The MAX phases are a candidate as potential materials used in fuel cladding applications due to their exceptional characteristics as bulky shape or coating materials [29].

Apart from cost considerations, the fuel cladding materials in nuclear applications must survive severe operation circumstances, such as thermal-mechanical stress, excessive irradiation with neutron dose, and extreme oxidation or corrosion surroundings [29]. High-purity MAX phases are required to exhibit favorable mechanical characteristics, compatibility with coolant (i.e., anti-oxidation along with anti-corrosion characteristics), and radiation tolerance for their application as nuclear fuel cladding [30].

Zr-metal MAX phases are considered non-superconducting with a low-temperature superconductor. As a result of the theoretical examination, the self-healing ability study and elevated temperature selective oxidation study of MAX phase (Zr_2AlC) can fulfil the fracture repair (cracks healing) requirements [29]. Fig. 3 shows the Zr_2AC crystal structures.

3. The MAX phase properties

The crystal structure of MAX phases is exhibited as hexagonal framework, belonging to the space group of $P6_3/mmc$. There are several different crystal structures for MAX phases, including 211, 312, 413, and 514, corresponding to n values of 1, 2, 3, and 4, respectively. Layer "A" always remains a constant in the MAX phase compounds, while layers "M" and "X" are separated with n as an essential factor (effect in physical properties). The unique mixture of characteristics may be attributed to their layered structure, where the layers of "X" are sandwiched between "M" layers and form MX blocks, which are joined by an individual layer of "A". This behavior is considered to significantly influence of the MAX phase's properties [32].

Moreover, the primarily metallic nature from the powerful bonds of M and X atoms (covalent as well as ionic) and the slight from the poor bonds of M and A atoms, especially in shear stress [33]. The high elastic stiffness of MAX phases results from the bond of M-X, while the metallic bond of M-A provides electrical and thermal conductivity characteristics. These bonds work together to give the MAX phases their distinct metallic-ceramic characteristics, as shown in Fig. 3. They exhibit several characteristics similar to those of metals, such as resistance to thermal shock (approximately to 1400 °C), plasticity deformation with high temperatures, easy machine,

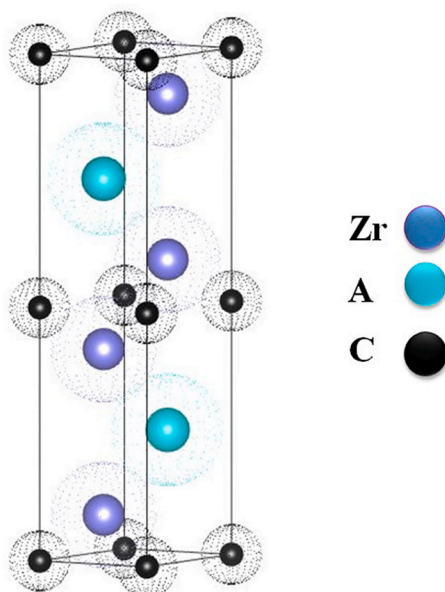


Fig. 2. The structure of the Zr_2AC MAX phase. * Drawing using the Materials Project website, Database version 2020_09_08. Powered by Pymatgen version 2022.0.8 and combined with the VESTA program (Visualization for Electronic and Structural Analysis ver.3.5.7, build data: Jan 7, 2021, copyright (c) 2006–2020 by Koichi Momma and Fuguo -Izumi).

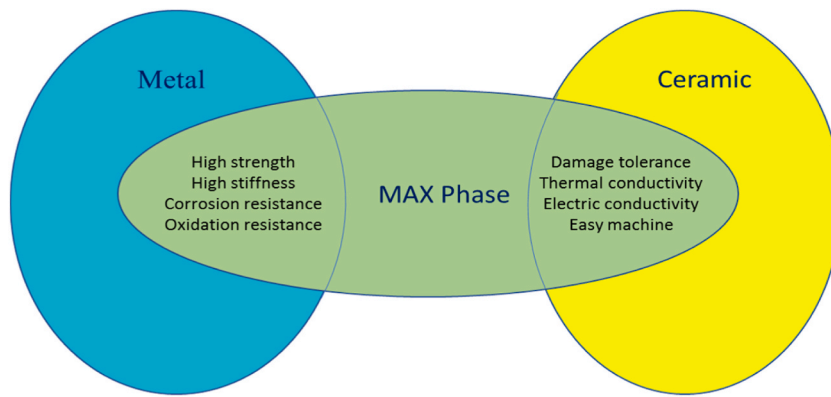


Fig. 3. Characteristics of the MAX phase ceramics [31].

and strong thermal plus electrical conductivity (usually greater compared to the equivalent pure metals). They are comparable to ceramics in terms of thermal expansion that are relatively light with high Young's modulus [34].

The MAX-phases exhibit notable mechanical distinctions compared to their binary counterparts, namely the MX carbides or nitrides. Furthermore, MAX phases possess more flexibility regarding their customization potential owing to three distinct intrinsic constituents. Adding atomic layers with different chemical compositions prevents dislocation motion (slide plane movement) and strengthens the composite material. Elastically rigid ceramics have high melting points, outstanding strength at elevated temperatures, small expansion coefficients, and high melting points. Furthermore, MAX phases are machinable, low-friction, and wear-resistant surfaces.

Conversely, the MAX phases resist corrosion, oxidation, fatigue, creep, and fracture. As a result, the MAX phases can apply in broad range. The combined properties of metal and ceramic were conducted, producing a macro scale, to the structural and electronically characteristics of the layers of atoms that comprise the nanoscale constituents [32,33,35,36].

3.1. The structural properties

The Zr_2AC MAX phases, where A is In, P, As, Tl, Si, Pb, Sn, Ge, or S, have a hexagon structure of crystal belonging to the $P6_3/mmc$ space group as well as contain 2 formula unit/cell; also, in the one-unit cell, there are eight atoms. The structure is characterized by 2 parameters of lattice a plus c , along with Z_M being the intern free coordinate of Zr atoms. In fact, the lattice constants of Zr_2AC max phase a , c , along with Z , could be determined by the experimental work. However, the experimental work calculation deviated from the theoretical study.

Another hand, the steric effect in the MAX phase can be explained by the atomic radius of M compared with the atomic radius of A element, indicating the quantity of distortion (Octahedron o_d and trigonal prism p_d distortion). The large M atoms mainly dominate the crystal structure. For example, if M atomic radius is larger compared with the atomic radius of A causes minimum distortion in both hydral-like (Zr and Sn), and if M atomic radius is smaller than the atomic radius of A causes significant distortion in both hydral-like (Nb, and Sn). It is worth noting that if the inter-parameter Z_M is very close to its ideal value, then the trigonal prism $[M_6A]$ is located at or very close to its ideal positions concerning the C planes [37].

Fig. 4 shows the structures of the Zr_2AC MAX phases. In these structures of the Zr_2AC MAX phase, four carbon atoms in its basic combined with one atom of zirconium, a transition metal belonging to a group 3–6, forming transition metal carbide. However, these carbides are separated by the A element layers, where A element can be Al, Si, P, S, Ge, As, Se In, Sn, Tl, Cd and Pb, denoted by different colors. The 211 crystal structure or Zr_2AC MAX phase with n equal to 1 according to formal $M_{n+1}AX_n$; therefore, there are two layers of A element separated zirconium carbide. In addition, the layer stacking sequence of the Zr_2AC structure across the c -axis can be described as C–Zr–A–Zr–C–Zr–A–Zr–C. Table 2 shows the structural parameters in order to display the differences in properties of the Zr_2AC MAX phase when the A element as the following: Al, Si, P, S, Ge, As, Se In, Sn, Tl and Pb. Also, the structure properties change with constant transition metal (Zr) and different A elements were represented (Al, Si, P, S, Ge, As, Se In, Sn, Tl and Pb). Furthermore, theoretical and experimental values for various parameters and properties of the Zr_2AC MAX phase are presented, including lattice parameters a and c , Z_M , o_d distortion, p_d distortion, B (GPa), TDOS at the Fermi level N (EF) in states/eV/Cell, and formation energy DEf. The numbers within brackets correspond to the experimental data. As seen in Table 2, the Zr_2AC lattice parameters a and c are deviation experimentally by 0.1–2% and 0.15–2.87% compared with the theoretical study.

3.1.1. The structural properties of the Zr_2AC MAX phase

The Zr_2AC MAX phases display a hexagonal crystal structure ($P6_3/mmc$ space group), with two formula units within each unit cell. The Zr, A, and C atoms are at $(1/3, 2/3, z)$, $(2/3, 1/3, 1/4)$, and $(0, 0, 0)$. The Zr_2AC has alternating blocks of zirconium carbide (Zr_2C) and networks of A atoms in its hexagonal closest packing. Fig. 4 (a-l) shows the Zr_2AC structure's layer stacking sequence along the c -axis: C–Zr–A–Zr–C–Zr–A–Zr–C. The Zr layer is present in every other layer, where the C atoms occupy octahedral voids or anti-crystal structures. Also, the Zr_2AC structural properties often match experimental results. Despite the Zr_2AC lattice parameters revealing slight deviation compared with experimental measurements [39,41,64].

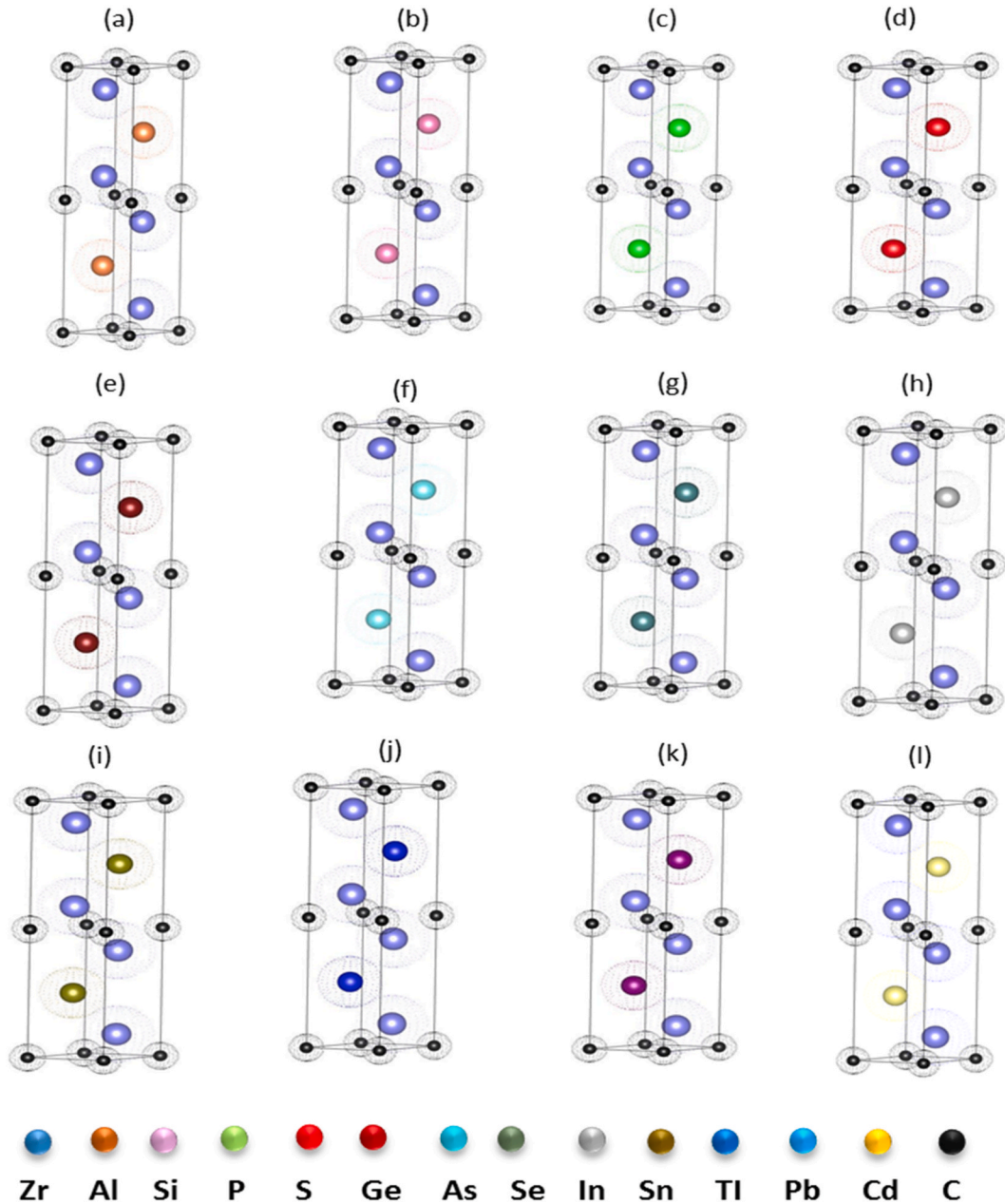


Fig. 4. The Zr_2AC ($A = Al, Si, P, S, Ge, As, Se, In, Sn, Tl, Pb$) crystal structural MAX phase where (a) Zr_2AlC MAX phase, (b), Zr_2SiC MAX phase, (c) Zr_2PC MAX phase (d) Zr_2SC MAX phase (e) Zr_2GeC MAX phase, (f) Zr_2AsC MAX phase, (g) Zr_2SeC MAX phase, (h) Zr_2InC MAX phase, (i) Zr_2SnC MAX phase, (j) Zr_2TlC MAX phase, (k) Zr_2PbC MAX phase, (l) Zr_2CdC MAX phase. * Drawing using the Materials Project website, Database version 2020_09_08. Powered by Pymatgen version 2022.0.8 and combined with the VESTA program (Visualization for Electronic and Structural Analysis ver.3.5.7, build data:Jan 7, 2021, copyright (c) 2006–2020 by Koichi Momma and Fuguo -Izumi).

Kanoun et al. (2010) found that in comparison to available experimental work, the Zr_2AC ($A = Pb, Si, Tl, Ge, P, S, Sn, As, In$) variation rates are predicted to be roughly 0.1% and 0.8% for a and c , respectively. The unit cell of MAX crystal comprises (M_6X) octahedra and (M_6A) triangular prisms when the valence electron density of the A atom is rising, leading to deformation in the two structural units of polyhedral. However, the triangular prism was further affected by this change (higher deformation) [64].

3.1.2. The structural properties of the Zr_2SnC MAX phase

The Zr_2SnC MAX phase contains a space groups notation of $P6_3/mmc$. Fig. 4(i) shows Wyckoff locations for atoms in the MAX phase. The carbon and tin atoms occupy the 2(a) and 2(d) locations at coordinates (0, 0, 0) plus (0, 0, 1/2), respectively, while the Zr atoms occupy the 4(f) positions with coordinates (2/3, 1/3, $z+1/2$), where Z_M is the inter free coordinate. For 4f atoms, Z_M must be 1/

Table 2

Lattice parameters a and c , Z_M , od distortion, pd distortion, B (GPa), TDOS at the Fermi level N (EF) in states/eV/Cell, and formation energy DEF. The numbers within brackets correspond to the experimental data in Table 2.

	A (Å)	C (Å)	C/A	V	Z_M	O_D	P_D	B	B^0	DEF	DEF	ref.
Zr ₂ AlC	3.308	14.680			0.08436	1.0792	1.0698	150.4	4.0	-0.726	-2.274	a [38]
	3.308	14.680			0.08436							a [39]
	3.3237	14.5705			0.0871							**c [29]
	3.3239	14.556			0.0898							**d [29]
	3.3237	14.5705										a [40]
Zr ₂ InC	3.319	14.606	4.400	139.312	0.0864			125	4.20		2.75	a [41]
	3.347	14.91	4.455									** [42]
								127 ± 5	4.25 ± 0.3			** [43]
	3.358	15.090			0.08123			117	4.4			a [44]
	3.35 (3.34)	15.04 (14.91)	4.49 (4.46)	146.62 (144.05)	0.0817			113			2.74	a [45]
	3.367	15.10 14.91										a [43]
	3.35											** [43]
	3.334 (3.34)	15.021 (14.91)			0.08640	1.0430	1.0680	147.95	4.212	-1.250	-2.431	a [38]
	3.3867	15.2403	4.5									e [28]
	3.3647	15.0742						126.03	4.074.22			f/g [46]
	3.3061	14.8044						138.02				h [46]
	3.36	15.11	4.49	148.036	0.0825							a [47]
Zr ₂ TlC	3.353 (3.36)	14.921 (14.78)			0.08147	1.1096	1.0565	148.73	3.234	-1.590	-2.152	a [38]
	3.3867	14.9016	4.4									e [28]
	3.15	13.98	4.42	119.64	0.0817			120				f [48]
	3.38	14.99	4.43	148.57								f [48]
	3.36	14.78	4.4	144.54								f [48]
	3.3241 3.3732	14.784	4.4475		0.0821			134	4.84			h [49]
Zr ₂ SiC		15.071	4.4678		0.0809			117	4.61			b [49]
	3.338	13.834			0.09215	1.0605	1.1461	172.8	4.20	-0.977	-2.651	a [38]
	3.338	13.834			0.09215							**c [39]
	3.309	13.653	4.126	129.49	0.0943			150	4.20		2.88	f [41]
	3.2778	13.624	4.156		0.0945			162.09	3.971			f [50]
Zr ₂ GeC	3.351	13.943			0.09051	1.0736	1.1368	170.0	4.222	-0.586	-3.767	a [38]
	3.3148	13.590	4.0999		0.0940			149	4.36			<u>a [51]</u>
Zr ₂ SnC	3.352 (3.357)	14.681 (14.57)			0.08500	1.0844	1.0811	156.0	4.441	-1.269	-2.721	a [38]
	3.2951	14.458			4.3844							<u>a [52]</u>
	3.3338	14.6687	4.4									e [28]
	3.352	14.681	4.38		0.0850	—	—	149	4.1	—	—	<u>a [37]</u>
		4.337										**c [53]
		4.341										**d [53]

(continued on next page)

Table 2 (continued)

	A (Å)	C (Å)	C/A	V	Z _M	O _D	P _D	B	B ⁰	DEF	DEF	ref.
Zr ₂ PbC	3.3576 ± 0.0005	14.568 ± 0.0003										**c [54]
	3.384 (3.38)	14.885 (14.66)			0.08330	1.0995	1.0715	148.3	4.3	-0.821	-1.965	^a a [38]
	3.3867	14.9016	4.4									^a e [28]
	3.41	14.96	4.39	150.60	0.0816							^a e,f [55]
Zr ₂ PC	3.413	14.868	4.356	150.02		1.1322	1.070				-2.940	^a e,f [16]
	3.433	12.173			0.10280	1.1044	1.2848	185.83	4.106	-1.213	-4.527	^a a [38]
	3.433	12.173			0.10280							^a a [39]
	3.450	12.210	3.572	125.874	0.1047			173	4.00		3.62	^a f [41]
Zr ₂ AsC	3.513	12.682			0.09286	1.1863	1.2354	159.20	4.15	-1.590	-6.700	^a a [38]
Zr ₂ SC	3.485	12.524			0.09741	1.1435	1.2558	162.66	4.113	-1.472	-1.300	^a a [38]
	3.485	12.524			0.09741							^a a [39]
	3.3663	12.0225	3.5714		0.1013			188	4.29			^a b [56]
	3.419	12.212	3.572	123.603	0.1008			166	4.40		1.38	^a f [41]
	3.406	12.14		122.0								** [57]
	3.4234	12.20						189 3.86	3.5637			^a a [58]
	3.411 3.402	12.152			0.1011			179.3	3.95			^a f [59]
		12.135			0.1016			185.5	3.90			^a h [59]
Zr ₂ SeC	3.427	12.195			0.1009			164	4.32			^a e,f [60]
	3.4655	12.5406	3.618	130.429								e,f [61]
	3.462	12.518										**c [62]
	3.487	12.631										^a a [62]
	3.491	12.556										**T [62]
	3.468	12.543		130.4								^a f [63]

A, FP-LAPW (full-potential linearized augmented plane-wave method); b, PP-PW (plane-wave pseudopotential); c, XRD (X-Ray Diffraction); d, NPD (Neutron Powder Diffraction); e, PBE (Perdew-Burke Ernzerhof formalism); f, GGA (energy functional used is the generalized gradient approximation); g, PW91 (Perdew-Wang's exchange-correlation function); h, LDA/CAPZ the localized density approximation for the Ceperly-Alder and Perdew-Zunger exchange-correlation function and T; TEM.

^a Theoretical, ** experimental.

12. Furthermore, The Zr_2SnC MAX phase has an alternating block of transition metal carbide made of edge-shared M_6C octahedrons and pure layers of A element in the unit cell [38,53,63]. However, **Bouhemadou (2008)** found that the lattice parameters c with a of Zr_2SnC exhibit a deviation of 2% compared to the observed lattice constant [52]. While, **Kanoun et al., (2009)** found that the deviation of c as well as a Zr_2SnC lattice constant are experimental obtaining as 0.76 and 0.15%, which is a slight deviation compared with **Bouhemadou (2008)**. In addition, a steric effect was observed at the M site. The Zr_2SnC polyhedra (trigonal prism and octahedron prism form the unit cell) exhibits lower deform than other M_2SnC like $M = Ti, Nb$ (atomic diameter similar than of Sn atoms) due to the atomic diameter of Zr bigger compared with the diameter of Sn [37].

3.1.3. The structural properties of the Zr_2InC MAX phase

The Zr_2InC MAX phase possesses a hexagonal crystal structure characterized by a space group of $P6_3/mmc$. The unit cell contains a pair of molecules and eight atoms, with four Zr atoms occupying the Wyckoff set at $(1/3, 2/3, ZM)$, carbon atoms at $(0, 0, 0)$, and In atoms at $(1/3, 2/3, 3/4)$, which can be visualized in Fig. 4(h). In fact, their determined results are compared to other published results and agree with them [43–47,52,65]. Moreover, it was observed that Zr_2InC exhibited a higher degree of compressibility along the c -axis compared to the a -axis [43,44]. Otherwise, **B. Manoun et al., (2004)** fabricated bulk polycrystalline samples of Zr_2InC by HIPS. The Zr_2InC MAX phase structure is stable even at high pressure of 52 Gpa. The ab initio calculated a (3.367) and c (15.100) parameters are likewise slightly bigger than the measured values ($a = 3.35$ and $c = 14.91$). Interestingly, hysteresis was discovered in the a lattice parameter, which was higher when unloaded than when its loaded. Also, the cause of this hysteresis is unknown recently [43]. The research study by **Medkour et al., (2008)** also found that the estimated Zr_2InC lattice parameters a and c differ from the observed by 0.27% and 1.20%, respectively. The determined volume of the Zr_2InC unit cell is approximately 1.78%, greater than the experimental readings [44]. This reflects mightily the finding of **He et al.,(2008)**, which calculated the lattice parameters values ($c, a, Z_m, c/a$, and V (volume of the unit cell)) with the deviation ratio of a and c constants of Zr_2InC from the experimental to be 0.3% and 0.9%, respectively [45]. Moreover, **Yang et al., (2013)** discovered that there is always ultra-incompressibility along the c -axis direction ranging from 70 GPa to 400 GPa in the Zr_2InC MAX phase. The core-valence charge transfer decreasing causes this unusual behavior. The rapid displacement of Zr atoms across the c -axis direction also resulted in ultra-incompressibility, which is greatly reduced beyond 400 Gpa [46]. Finally, **Sultana et al., (2018)** found that Zr_2InC lattice constant deviation a and c to be 1.34% plus 0.3% greater than the experimental values, respectively [47].

3.1.4. The structural properties of the Zr_2PbC MAX phase

The Zr_2PbC MAX phase exhibits a hexagonal crystal structure, characterized by the $P6_3/mmc$ space group, as shown in Fig. 4(k). The structure consists of ZrC layers stacked in a close-packed manner and interspersed by a layer of Sn every 4 layers, as illustrated in Fig. 4(k). The carbon atoms are positioned at $2a$ $(0, 0, 0)$, Pb atoms at $2d$ $(1/3, 2/3, 3/4)$, with zirconium atoms at $4f$ $(1/3, 2/3, z)$, whereby $Z_m = 0.083$, as well as the unit cell containing 8 atoms and 2 formula units. The computed structural parameters good agree with the identified theoretical and experimental results at zero pressure [16,55,66]. **Qian et al.,(2012)** obtained that the deviation of Zr_2PbC lattice constants a as well as c is about 0.7% and 1.8%, respectively, compared with the experiment results [66]. In comparison, **Khatun et al.,(2020)** identify that lattice constants and unit cell volume drop almost linearly when applied pressure increases on the Zr_2PbC lattice. On the other hand, the hexagonal ratio c/a progressively increases with increased pressure (0 to 100 Gpa) to a ratio of 4.1%. This observation implies that the lattice constant " a " exhibits a more rapid decrease than the lattice constant " c ". Consequently, the degree of compressibility exhibited along the c -axis ($c/c_0 = 9.1\%$) is lower than along the a -axis ($a/a_0 = 12.8\%$) coupled with normalized volume (V/V_0) decreased to 30.8% as shown in Table 3 with Fig. 5(a–d) [55]. Fig. 5(f) shows the internal parameter Z_m of the Zr_2PbC MAX phase with applied pressure [55]. **Alrebdy et al.,(2021)** indicated that the calculated deviations of the MAX phase Zr_2PbC experimental values for lattice constants c and a were 2.87% plus 0.88%, respectively, which is not coincide with **Qian et al., (2012)**. They also observed distortion of the two polyhedra (octahedra (M_6X) and trigonal prisms (M_6A)) of the MAX phase. Although this distortion of polyhedra is low in the Zr_2PbC MAX phase compared to the Ti_2PbC MAX phase due to it has a large Zr atomic radius. Furthermore, the steric effect can be referred to as this behavior, where the M atom formed as a big portion of the topology of the structure of lattice. The steric effect is further characterized via observation that the lattice parameters c plus a for Zr_2PbC that were bigger than those in Ti_2PbC MAX phase [16].

Table 3

The theoretical calculations of the lattice constants, including ($a, c, c/a, Z_m$) and volume of the unit cell (V) of the Zr_2PbC MAX phase at (0–100) P (Gpa) Pressures [55].

Pressure	a	c	c/a	Z_m	V	a/a_0	c/c_0	V/V_0
0	3.41	14.96	4.39	0.0816	150.60	1	1	1
20	3.26	14.40	4.41	0.0852	132.66	0.95	0.96	0.88
40	3.16	14.10	4.46	0.0869	122.15	0.92	0.94	0.81
60	3.09	13.90	4.50	0.0881	114.63	0.9	0.92	0.76
80	3.03	13.74	4.54	0.0888	108.86	0.88	0.918	0.72
100	2.97	13.60	4.57	0.0893	104.16	0.87	0.909	0.69

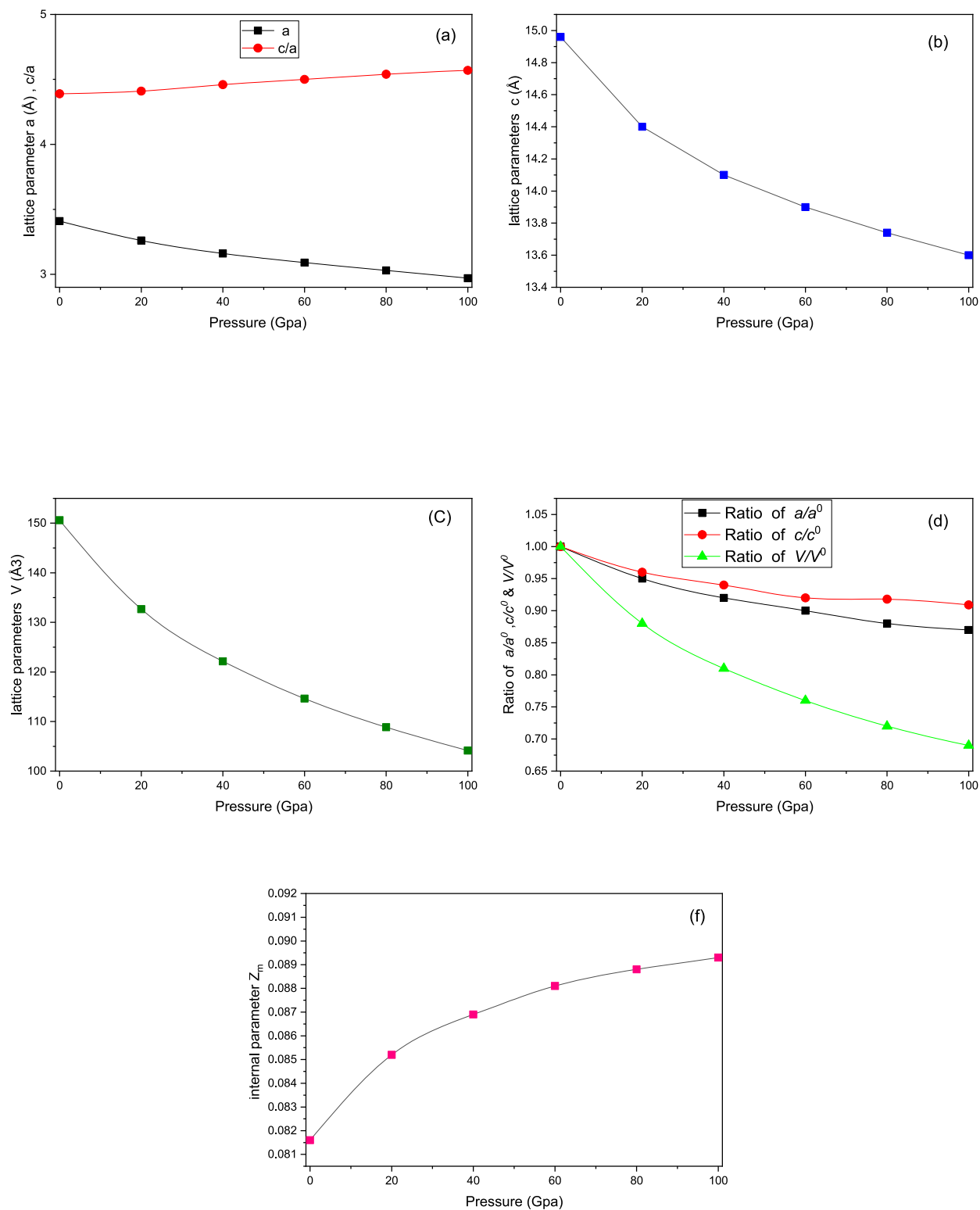


Fig. 5. Zr₂PbC structure parameters with pressure dependence (a) lattice constant a and ratio c/a (b) lattice constant c (c) volume of the unit cell V (d) normalized lattice parameter c/c_0 plus a/a_0 with the volume of unit cell V/V_0 and (f) The Z_m with operating pressure relation [55].

3.1.5. The structural properties of the Zr_2SC MAX phase

The Zr_2SC MAX phase exhibits a hexagonal crystal structure belonging to the $P6_3/mmc$ space group. It has only 8 atoms in a one-unit cell, which can be observed in Fig. 4(d). Furthermore, the sites $(1/3, 2/3, z)$, $(2/3, 1/3, 1/4)$, plus $(0, 0, 0)$ are occupied by zirconium atoms, sulfur atoms, and carbon atoms, respectively [56,58,59]. Also, Bouhemadou et al., (2008) obtained that the deviation of a and c of the Zr_2SC MAX phase compared with the experimental results is about 1% and 0.88%, respectively as well as the calculated c/a ratio is 0.10% that, is larger than the experimental values [56]. Indeed, Fu et al., (2009) found that the most stable structure of the Zr_2SC when the lattice parameters c with a were 12.103488 Å and 3.389331 Å, respectively, as well as the axial ratio c/a , is 3.571. These agree closely with experimental values. The calculated percentage of V/V_0 , a/a_0 , and c/c_0 , are changed depending on pressure, and the a -axis has a linear compressibility that is roughly 1.22 times greater than the c -axis. The compression along the c direction in Zr_2SC is smaller than along the a axis, making it unique among MAX phases; this finding suggests the fact that M-A (Zr-S) bonds are stronger compared with the M-X (Zr-C) bonds [58].

3.1.6. The structural properties of the Zr_2SeC MAX phase

The Zr_2SeC MAX phase possesses a hexagonal structure characterized by the $P6_3/mmc$ space group, as illustrated in Fig. 4(g). There are 8 atoms within the unit cell, formed by combining two formula units. Fig. 4(g) shows the Zr_6C octahedron between two selenium atomic layers. The unit cell atomic locations of zirconium, selenium, and carbon in 211 MAX phases are $(0, 0, 0)$, $(1/3, 2/3, 3/4)$, and $(1/3, 2/3, 0.0965)$ [61,63]. Particularly, Ali and Qureshi (2021) observed structural parameters that are consistent with the previous findings. However, the obtained value of V , c , as well as a is 1.08%, 0.182%, and 0.1% larger compared with the experimental results [61]. Furthermore, the Zr_2SeC MAX phase is characterized by a decrease in lattice parameters with increasing pressure (0-25) GPa and a corresponding decrease in volume, as indicated by Akhter et al., (2022). In addition, its compression across the a axis was higher compared with that across the c axis, which was apparent from the faster reduction in the lattice parameters due to the pressure compared to the c axis. As applied pressure, the volume is compressed, leading to a drop in both a/a_0 and c/c_0 [63]. Table 4 shows the lattice parameters and unit cell volume of the Zr_2SeC MAX phase in (0–25) Gpa pressure [63].

3.1.7. The structural properties of the Zr_2TiC MAX phase

The Zr_2TiC MAX phase is a hexagonal structure as in the $P6_3/mmc$ space group, which can be visualized in Fig. 4(j). The unit cell consists of eight atoms and is made up of two formula units. The atomic Wyckoff sites for Ti are 2(a) $[(0, 0, 0), (0, 0, 1/2)]$. For the c , the sites are 2(d) $[(1/3, 2/3, 3/4), (2/3, 1/3, 1/4)]$. Lastly, for M (where M represents Ti, Zr, or Hf), the sites are 4(f) $[(1/3, 2/3, z), (2/3, 1/3, z+1/2), (2/3, 1/3, -z), (1/3, 2/3, -z+1/2)]$, with Z being the internal free coordinate. However, the existing experimental data and the results of the structure parameter of the unit cell of the Zr_2TiC MAX phase are in reasonable agreement with the literatures [48,49]. Moreover, Warner et al., (2006) indicated that the Zr_2TiC MAX phase percentage differed among the experimental and calculated results of c and a to be 1.4% and 0.6% [48]. Bouhemadou (2009) discovered that the Zr_2TiC MAX phase deviation is calculated a and c from the experimental work to be 1.0 and 0.0% (0.4 and 1.9%), respectively. From the present study, these findings are in excellent agreement with the findings of Warner et al., (2006). Also, the difference of c/a value of the Zr_2TiC MAX phase with the experimental work is 1.0 to be 1.5%. When the lattice constants are subjected to high pressures up to 20 Gpa, the a -axis direction was subject to lower contractions compared to the c -axis [49].

3.1.8. The structural properties of the Zr_2GeC MAX phase

Bouhemadou (2009) found that the Zr_2GeC MAX phase is a hexagonal structure with the space group of $P6_3$ per mmc as displayed in Fig. 4(e). The Zr_2GeC unit cell consists of two unit formulas. In this structure, the atomic Wyckoff site for carbon is located at the $(0, 0, 0)$ position. The germanium atoms occupy the $(1/3, 2/3, 3/4)$ sites, while the M atoms (representing Ti, Zr, or Hf) are found at the $(1/3, 2/3, z)$ positions. In fact, the unit cell geometry optimizations is agree with current experimental results [51].

3.1.9. The structural properties of the Zr_2SiC MAX phase

The hexagonal structure of the Zr_2SiC MAX phase, belonging to the $P6_3/mmc$ space group, is illustrated in Fig. 4(b). The atomic locations of carbon, silicon, and M are $(0, 0, 0)$, $(1/3, 2/3, 3/4)$, and $(1/3, 2/3, Z)$, respectively. The Lattice constants must be increased because the M atoms are large in size, and when the VEC (valance electron concentration) of M atoms rises, the lattice constants drop simultaneously [50].

Table 4

The theoretical calculations of the lattice parameters and unit cell volume of the Zr_2SeC MAX phase in (0–25) Gpa pressure [63].

Pressure	a	c	V
0	3.468	12.543	130.4
	3.462	12.518	132.66
	3.487	12.631	132.1
5	3.430	12.429	126.7
10	3.396	12.334	123.2
15	3.366	12.252	120.3
20	3.339	12.181	117.6
25	3.315	12.114	115.3

3.2. Electronic properties

The MAX phases' electronic structure has been subjected to extensive theoretical investigation. The research summarizes the 211 MAX bond pattern in the following manner: The M *d*-A *p* bond was relatively weak beneath the Fermi level (EF), while the M *d*-X *p*, as well as M *d*-X *s* bonds, were strong (deeper in energy). The MAX phase obtained a metallic character, but the conductivity varies between the different types of MAX phases. Also, at EF the DOS is not proportional to movements of charge carriers (including holes and electrons) in these materials, excepting the Ti₄AlN₃. This trend is observed in other MAX phases [37].

The essential link between the crystal structure as well as the physical characteristics of the solid crystal is the calculation of the electronic band structure. It thoroughly explains many of these characteristics, including charge transport, electrical resistivity, optical absorption, and optical properties of MAX phases [55]. Table 5 illustrates the electronic characteristics of the Zr₂AC MAX phases.

3.2.1. The electronic properties of Zr₂SnC MAX phase

Several studies have highlighted the unique properties of this ternary layered MAX phase, including its excellent electrical conductivity. The electrical conductivity (σ) of the Zr₂SnC MAX phase exhibited characteristics of a metallic behavior demonstrated a direct correlation with temperature reduction, indicating a linear increase in its performance [54,67]. The DOS of the Zr₂AC MAX phase is primarily made up of Zr *d* states, with the electronic structures being close to the Fermi level. The Stabilizing of the Zr₂AC structures (the structure's driving force) is achieved through the development of covalent Zr-A and Zr-C bonds, as well as the strong Zr *d*-C *p* hybridization. The bonding characteristics observed in the Zr₂AC MAX phases can be described as a combination of metallic, covalent, and ionic interactions. This is attributed to the differing electronegativities of the constituent elements and the presence of ionic bonds.

Moreover, there is a connection between Sn *5p* states and M *d* states. These M *d*-Sn *p* hybrids' energy levels are higher than the M *d*-C *p* hybrids, with a difference of approximately four states eV-1 per cell. This observation is attributed to the significantly more powerful bonding of M - C compared to M-Sn. The stability of the M₂SnC structure is due to its powerful M *d*-C *p* hybridization. Despite the competition with weaker M - Sn hybrids, the powerful M *d*-C *p* hybridization stabilizes the M₂SnC structure, resulting in non-cubic distortions for polyhedra such as octahedra and trigonal prisms [37,39,41,68].

Barsoum et al., (1997) determined the conductivity of Zr₂SnC to be equivalent to $(7 \times 10^6) (\Omega.m)^{-1}$ and demonstrated its good electrical conductivity at room temperature [54]. El-Raghy et al.,(2000) also fabricated a fully dense single phase of Zr₂SnC (92 ± 94 vol%) and reported the Zr₂SnC as a good electrical conductor, with a conductivity of about $3.57 \times 10^6 (m \Omega)^{-1}$. They found the electrical conductivity is very high (~1/3 of Al metal). The Zr₂SnC MAX phase has a temperature coefficient of resistivity of 0.0035 (k⁻¹) [67]. In addition, while the Poisson ratio (ν) for covalent materials is 0.1 and for ionic materials is 0.25, the Poisson ratio (ν) for M₂SnC is 0.214–0.215, suggesting a significant ionic involvement in atomic bonding. Moreover, the calculated G/B percentage is (0.6–0.79) from an experiment by Kanoun et al., (2009) suggests that the combined covalent -ionic bonding is correct for M₂SnC [68]. Kanoun et al., (2010) calculated G/B (0.6–0.79), which also indicates that the mixed ionic-covalent bonding is suitable for M₂SnC [38]. Kang (2013) provides a deep analysis of the electronic structure and elastic characteristics of layered Zr₂AC (A = Si, Al, S, P) carbides which depend on the *p* state occupying of (A) element. They found the Zr-A bonds strengthened gradually, as the A *3p* state occupied increased as in Zr *4d* - A *3p* bonding states placed deep in energy (below the Fermi level). Furthermore, the sulfur occupied the high *p* states of A element in the Zr₂AC MAX phase, suggesting that Zr-S bonds might be as strong as Zr-P bonds. However, the Zr-S bond in Zr₂SC is weaker than the Zr-P bond in Zr₂PC due to a wide gap between zirconium and sulfur, and it decreases as coupling overlaps. This increases negativity, contributing to the elasticity of the Zr₂SC MAX phase. Most MAX phases have a finite value of the DOS at EF, and it is not exhibit a band gap. This result provides further evidence that these materials are metallic compounds.

All Zr₂AC structures compress the Zr₆C octahedra along with the Z. The Zr₂AlC MAX phase has 3.31 Å in-plane and 3.13 Å interlayer Zr-Zr distances, compared with bulk zirconium metal's 3.17 Å Zr-Zr distance. As a result, bonding must depend on zirconium atom d-d interactions in the Zr₂C sub-lattice. The Zr-C bond in ternary carbides (2.28 Å) is smaller than in binaries (2.35 Å), suggesting strong orbital interactions between zirconium and carbon. Thus, the ternary carbides preserve strong Zr-C bonds. The Zr-Al length is 3.09 Å, while the sum of Zr and Al's single-bond metallic radii (2.70 Å) is much smaller than this distance. This suggests a weaker Zr-Al interaction than Zr-C. The Zr₂AlC MAX phase has a considerably greater Al-Al bond distance (3.31 Å) than pure Al (2.86 Å). Also, the Al atoms attach to Zr₆C blocks via *p*-*d* overlapping outside the basal planes, as well as its not made formed bonding between them. The Zr₂SiC MAX phase overlaps much more than the Zr₂AlC MAX phase. Fig. 6(b) shows the DOS of the Zr₂SiC MAX phase.

Zr₂AlC and Zr₂SiC MAX phases have comparable band structures. Nevertheless, the Zr *4d*-Si *3p* bonding states, ranging from -12.5 to -11 eV, as illustrated in Fig. 6(b). They moved to lower energy compared to the Zr *4d*-Al levels at -11 eV to -10 eV as displayed in Fig. 6(a). This suggests greater bonding strength of Zr-Si in the Zr₂SiC MAX phase versus Zr-Al in the Zr₂AlC MAX phases.

Table 5
The theoretical calculations of the state's position of Zr₂InC (C-*p* and C-*s*) [45].

Zr ₂ InC	C- <i>s</i>	C- <i>p</i>
Bottom (eV)	-10.63	-9.04
Top (eV)	-5.08	-2.01

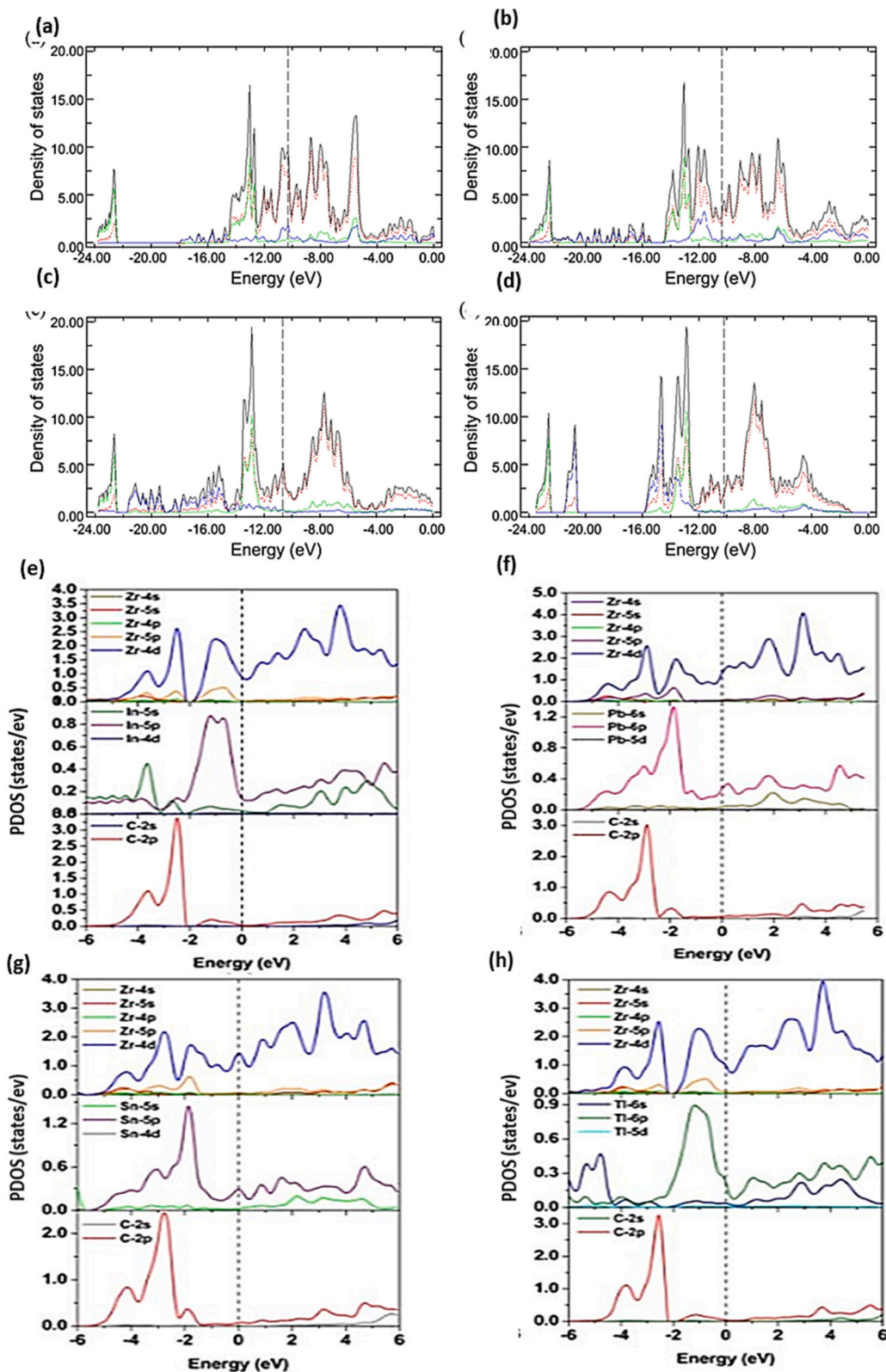


Fig. 6 (a–d). TDOS by Kang (2013) where A (blue line), C (green line), and Zr (red line) orbitals at (a) Zr₂AlC, (b) Zr₂SiC, (c) Zr₂PC, and (d) Zr₂SC [39] and DOS of MAX phase by Ahms et al., (2020) (e) Zr₂InC (f) Zr₂PbC (g) Zr₂SnC (h) Zr₂TiC [28]. Vertical lines with dashes indicate EF. (For interpretation of the references to color in this figure legend, the reader is referred to the Web version of this article.)

Furthermore, the Zr–C–Zr slab's d-d interactions between Zr atoms cause metallic bonding levels (states) near the EF which shear little in the bonding. The Zr₂PC bonds differently from Zr₂SiC as the A-group element shifts from Si → P. This implies a stronger Zr–P bond than the Zr–C bond. MAX phases rarely have strong M–A bonds. This must improve Zr₂PC's phase stability with structural and mechanical characteristics. The Zr–P distance is 2.67 Å, somewhat higher than a Zr–P single bond's 2.55 Å. Hence, these orbitals can overlap strongly. This interaction is sizable despite a large energy gap between the orbitals. The strong of the Zr–P bonds give Zr₂PC a high B and its boost the strength. The Zr₂SC and Zr₂PC MAX phases achieved slightly different electrical structures. As seen in Fig. 6(c, d), S 3p orbitals have a narrow partial density of states (PDOS) from –16 eV to –14 eV due to it has less mixing with Zr 4d orbitals since Zr and S atoms to be 2.78 Å. Also, the Zr–S bond has a greater bond distance than Zr–P despite the S atoms has smaller covalent radius. The Zr–S bond is weaker than the Zr–P bond due to its longer bond distance that lowers Zr₂SC's elasticity [39]. Additionally, Nasir et al., (2014) studied the electronic structures of Zr₂AC (A = Al, Si, P, S), with partial and total density of states of the Zr₂AC(A = Al, Si, P, S) MAX phase [41]. Again, Ahams et al., (2020) indicated that the bands considerable hybridization of the energy states from the valence to the conduction bands. The density of states (DOS) calculated and band structures data reveal that Zr₂AC (where A is In, Sn, Pb, and Tl) MAX phase has no band gap or zero band gaps. This behavior indicates that the MAX phases are metallic conductors. The calculated DOS shows that Zr₂SnC seems to have the largest DOS of the four phases. Three energy zones have been created: (I) The lowest energy zone is –6 to –2 eV. Many energy states hybridize in this zone, including Zr-4d, Pb-6p, Sn-5p, In-5s, C-2p, and Tl-6s covalent structure. (ii) Zr-4d dominates the valence energy domain from –2 to 0 eV, with a modest contribution by In-5p, Sn-5p, Pb-6p, and Tl-6p. (iii) From 0 eV (EF) to the conduction band, Zr-4d, Sn -5p, In -5p, Pb -6p, and Tl-6p dominate. Zr₂SnC has the greatest DOS, and Zr₂InC has the lowest. The Zr-4d and In-5p, Tl-6p dominate the valence band plus lower conduction band, whereas Pb-6p, Sn-5p, and C-2p dominate the minimum energy zone for each phase. Moreover, the Zr -4d energy states dominate the energy states of (–6 eV – 6 eV) around EF (through the three energy zone). Thus the Zr-4d is the basis of the conduction properties of MAX phases. Multiple hybridizations are common through the three energy zone. Also, the DOS at the EF is unaffected by the four MAX phases' C-2p states. The computed density of states (DOS) for Zr₂InC, Zr₂PbC, Zr₂SnC, and Zr₂TlC is 1.151 states/eV, 1.783 states/eV, 1.951 states/eV, and 1.355 states/eV, respectively. Fig. 6(e-h) illustrates the DOS of MAX phase Zr₂InC, Zr₂PbC, Zr₂SnC, and Zr₂TlC [28]. On the other hand, Qureshi et al., (2022) manufactured metallic, anisotropic MAX phase with terminated surface. The bulk charges density of valance A-p electrons differs from the surface area in the most stable termination, which differs from that of the bulk. The higher DOS number of EF distinguishes terminated surfaces from bulk counterparts. Furthermore, the determined cleavage energies of M – C as well as M–A bonds confirm the PDOS's finding that M – C bonds are greater than M–A bonds because of the powerful hybridization among M d-C p orbitals. Results show that M–A bonds have lower cleavage energies and are easier to break than M – C bonds. The relaxation of the terminated surface shows that surface structures differ from bulk structures. Since electron coupling is stronger between surfaces and sub-surfaces, top surfaces relax inwards and sub-surfaces relax outwards. Finally, According to surface energy information, A-along with M(C)-terminated (0001) surfaces are most stable [69]. Fig. 7 shows the calculation of TDOS at EF as an indicator of Zr₂AC MAX phase A element electrons as a number of p [38].

3.2.2. The electronic properties of Zr₂InC MAX phase

Medkour et al.,(2008) found that there is no gap and vicinity at the EF of Zr₂InC; and, the overlap bonds and anti-bond states make the Zr₂InC structure stable. Furthermore, Zr₂InC exhibits metallic properties with 2.42 states/eV DOS at EF. Also, carbon is not

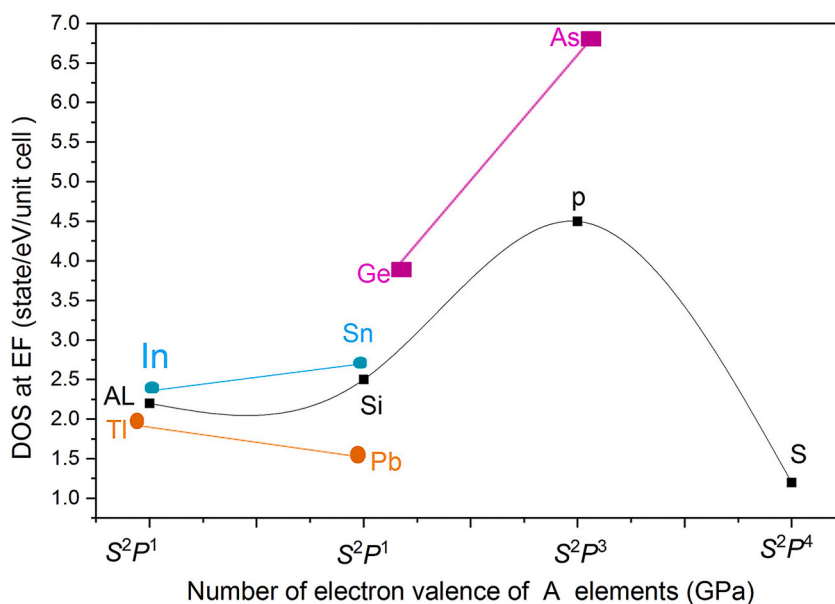


Fig. 7. The TDOS at EF as an indicator for electrons (e) a number of p orbital of the A element of Zr₂AC MAX phase [38].

contributing to the DOS of the Fermi level; hence it is not affect conduction characteristics, while Zr *d* electrons contribute to the DOS of EF as well as conductivity characteristics. The Zr₂InC MAX phase is an electrical conductor because the C *p* level hybridizes with the Zr *d* level to form strong directed bonds between Zr and C atoms. The hydrostatic pressure influence on bond lengths indicated that C-M along with In-M bonds, where M is (Hf, Ti, Zr) weaken in the order of Hf₂InC→Ti₂InC→Zr₂InC [44]. He *et al.*, (2009) also indicated that the Zr₂InC is conductive with 2.74 states/eV TDOS at EF. The DOS is generated by M-*d* levels close to the EF. Additionally, transition metal *d* bands govern electrical transport. The M₂InC MAX phase is theoretically investigated, showing that Zr₂InC achieved the smallest B due to a lower covalent connection between C-*s*, C-*p*, and M-*d* levels, as displayed in Table 5. The C-*p* plus M-*d* bonds were stronger than both In-*p* plus M-*d* [45]. The research study by Li *et al.*, (2022) found a strong M *d-p* X hybridization in the Zr₂InX MAX phase assisting to keep their crystal structure [65].

Furthermore, Sultana *et al.*, (2018) claimed that the Fermi level conduction-valence band overlap indicates metallicity along with electrical conductivity anisotropy indicated by lower *c*-axis energy dispersion. Otherwise, the electric conductivity was extending in the direction of the *ab*-plane compared with the *c*-axis direction. Also, the EF of Zr₂InC is not have a band gap because of the conduction-valence band overlap, and the TDOS of Zr₂InC is 2.4 states/eV at EF. The Zr-4*d* electrons are responsible for electrical conduction. Although, indium with carbon atoms shares minimally with the TDOS at the EF while failing to considerably contribute to the conduction band. Moreover, C-Zr > In-Zr bonds in the Zr₂InC MAX phase and these MAX phases have a strong covalent bond [47].

3.2.3. The electronic properties of Zr₂PbC MAX phase

The Zr₂PbC MAX phase is an excellent electrical conductor [66,70]. The M₂PbC MAX phases stability comes from Pb *p* -M *d* as well as C *p* -M *d* bonds. The C *p* -M *d* hybridization with less energy as well as stiffer bonding compared with Pb *p* -M *d* due to using the Pb element in its structure with the highest saturated *p* states. Also, the electronic structure at the EF shows that M *d* states dominate DOS and that M *d*-C *p* along with Pb *p* -M *d* hybridizations occur below EF. Also, a weak Pb *p* -M *d* with strong C *p* -M *d* hybridizations were found under EF. The charge density distribution demonstrates that the M and C atoms achieve a powerful M-C-M covalent bond chain. The Zr₂PbC MAX phase is an ionic-covalent-metallic character. The Mulliken atomic or charge density map calculation suggests that these MAX phases' bonding behavior may be a mixture of covalent-ionic and metallic bonds. The M-M covalent bonding was weaker than M - C, which agrees with Qian *et al.*, (2012), Khatun *et al.*, (2020), and Alrebdy *et al.*, (2021) Ahams *et al.*, (2022) [16,55,66, 70]. El-Raghy *et al.*, (2000) also fabricated a fully dense single phase of Zr₂PbC (92 ± 94 vol%). The Zr₂PbC MAX phase conductivity is about 2.77*10⁶ (m Ω)⁻¹. The temperature coefficient of resistivity of the Zr₂PbC MAX phase is 0.0144 (K⁻¹). The electrical conductivity is very high (~1/3 of Al metal), and (σ) displayed metallic behavior due to rising linearly as temperature decreased [67]. However, Qian *et al.*, (2012) indicated that for M₂PbC MAX phases where M is Hf, Zr and Ti), the DOS of Fermi energy falls as M atomic number rises [66]. On the other hand, Khatun *et al.*, (2020) observed that Zr₂PbC is metallic and exhibits zero band gap around the EF. Also, the DOS decreases with increasing pressure, as shown in Fig. 8 [55].

Furthermore, Ahams *et al.*, (2022) studied the electronic bands and TDOS, which show that Zr₂PbC ternary MAX phase has metallic characteristics. The Zr 4*d* and Pb 6*p* states are the primary contributors to the energy bands at the EF and another place in the vicinity. Also, the Zr - Pb hybridizations occur slightly below the EF and reach the conduction band, affecting more than the Zr-C bond. This finding is consistent with the findings in the previous studies mentioned above. The phonon influence on the thermal conductivity at finite temperatures was lower than the electron contribution.

Furthermore, the estimated transport coefficients show that replacing Zr with V increased the thermoelectric merit from 0.026 for Zr₂PbC to 0.13 for V₂PbC. The V₂PbC MAX phase has higher Seebeck coefficients (a material's Seebeck effect-induced thermoelectric voltage in responses to a temperature difference [71]) and ZT (The thermoelectricity efficiency, or ZT, is a dimensionless quantity) than Zr₂PbC as well as future thermoelectric materials. Due to their electrical conductivity, these MAX phases may be high-temperature conductive [70].

3.2.4. The electronic properties of Zr₂SC MAX phase

Bouhemadou (2008) observed that the Zr₂SC MAX phase conducts materials from the band structures. At the Fermi level (EF), the DOS depended on the transition metal's atomic number for the M₂SC MAX phases (M is Hf, Zr, or Ti). It decreases with an increased M atomic number (opposite relation).

Furthermore, the M-atom *d* state hybridized on C as well as S -atom *p* levels creating the bonding between atoms. The Sp-M*d* bonds are stronger and have less energy compared with Cp-M*d* bonds. The Zr₂SC MAX phase has lower conductivity than the Ti₂SC MAX

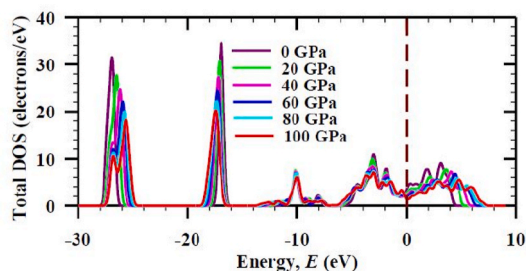


Fig. 8. The DOS under pressure at 0–100 Gpa, EF is the vertical dotted line [55].

phase, while it is higher than that of the Hf_2SC MAX phase [56]. **Feng et al. (2010)** also found that the equation of state (EOS) calculation of the Zr_2SC MAX phase agreed with the new experimental research. Furthermore, the Zr_2SC MAX phase is a metallic compound because of the band gap is absent on the EF. The pseudo gap and significant hybridization of $\text{Zr}4d$, $\text{S}3p$, and $\text{C}2p$ states stabilize the Zr_2SC MAX phase. The Zr_2SC MAX phase is brittle based on the bulk-shear modulus ratio. However, the Zr_2SC 's mechanism of brittleness comes from the massive Zr atom that occupies the internal Z parameter [59].

3.2.5. The electronic properties of Zr_2SeC MAX phase

The Zr_2SeC and Zr_2SC MAX phases show metal-like conduction because their conduction as well as valence band overlaps at the Fermi level (EF) [61–63]. **Ali and Qureshi (2021)** showed by studying the PDOS that Zr-d states dominate electrical conductivity and anisotropic behavior in c axis direction. Indeed, the DOS peak shifted due to selenium being replaced by sulfur, along with Zr_2SeC bonding weaker than Zr_2SC bonding as a result of the mapping (CDM) of charge density [61] while **Chen et al., (2021)** compared the electronic characteristics of both Zr_2SeC and Zr_2SC MAX phases and reported the temperature electric resistance of Zr_2SC ($1.75 \mu\Omega \text{ m}$) lower than Zr_2SeC ($1.57 \mu\Omega \text{ m}$). The Zr_2SeC 's TDOS was 1.48 states/eV, greater than that of Zr_2SC 's 1.36. Furthermore, the Zr_2SeC and Zr_2SC MAX phases achieved the greatest DOS at EF from 4 d electrons to Zr. The contribution of s and p orbitals electrons(e) from selenium, as well as at the EF, sulfur in TDOS (the total density of states), was initially minimal or negligible. However, their contribution became significant in the energy of approximately ($-6.7 \text{ eV} - -1.7 \text{ eV}$), resulting in bonding creation among zirconium and its chalcogen atoms (powerful interacting of Zr $d - p$ electrons). Zr_2SC also had higher density of electrons (charge-density difference) surrounding its S-atoms compared to Zr_2SeC given that the Zr–S bonds is tighter compared to the Zr–Se bonds. Finally, the strong binding strength improves phase stability and physical property tuning [62]. **Akhter et al., (2022)** also reveal metal-like conduction due to energy-dependent DOS as well as the structure of the electronic band. The Zr_2SeC 's metallic nature stays unaltered at pressure of 0–25 Gpa [63]. Finally, **Wang et al.,(2022)** reported that according to the powerful S-M bonds, the sulfur MAX phase (Hf_2SC plus Zr_2SC) had fewer thermal expansion coefficients (CTEs) than that of the selenium MAX phases (Hf_2SeC plus Zr_2SeC) [72].

3.2.6. The electronic properties of Zr_2TlC MAX phase

The band structures show that the Zr_2TlC MAX phase is conducted. Also, M_2TlC , (where M is, Hf, Ti Zr) shows that DOS at the EF is reducing with the atomic number of the M rising (opposite relation). The local density of states (LDOS) indicates that M atomic numbers increase carbon p electron involvement in C p and M d bond for M_2TlC (where M is, Hf, Ti Zr). The M d and carbon p have hybridization peaks of (-2 to -3 eV), while M $d - \text{Tl} p$ have (-1 to -2 eV). As a result, the M $d - \text{C} p$ bonds are greater compared with the M $d - \text{Tl} p$ bonds, as demonstrated by **Warner et al., (2006)** [48]. The research finding by Bouhemadou (2009) is also points to the idea that the Zr_2TlC is an electrical conductor due to band structures. The Zr_2TlC bonds result from hybridizations of M $d - \text{Tl} p$ and M $d - \text{C} p$ as revealed by the analysis of electronic structure. Furthermore, the M $d - \text{C} p$ bond has less energy and is stronger than the M $d - \text{Tl} p$ bond [49].

3.2.7. The electronic properties of Zr_2GeC MAX phase

Bouhemadou (2009) observed from the band structures that the Zr_2GeC MAX phase is electric conductor material. Additionally, the hybridizations of M $d - \text{C} p$ and M $d - \text{Ge} p$ are responsible for the bonding phenomenon, as shown by the position with the projected momentum investigation's densities [51].

3.2.8. The electronic properties of Zr_2SiC MAX phase

Ghebouli et al.,(2015) used the PDOS analysis to reveal powerful hybridizations between Si-M and M-C. Additionally, they investigated M_2SiC (where M is, V, Ti, Zr Cr, Mo, Nb, Hf, W, and Ta) MAX phase and showed that this MAX phase is an electric conductor, and the transition metal electrons (s orbital) generated the conductivity [50].

3.3. Mechanical properties

Elastic characteristics affect several principle parameters, involving Debye temperature, thermal expansion (TEC), specific heat, equations of states, melting point (T_m), and Gruneisen parameter. Indeed, the understanding of crystalline solid elastic behavior is crucial to pay attention to its brittleness, stability, hardness, ductility, bond properties among neighboring atomic planes, elasticity, anisotropy, as well as other mechanical properties. However, the elastic moduli and lattice constants supply most of this knowledge [55]. The elastic stiffness defines the crystal's response to external strain (or stress), giving data on bonding, mechanical, and structural stability. Also, the bulk modulus resists fracture, while the shear modulus resists plastic deformation [38].

M_2AC MAX phases are separated in to 2 categories as the following:

1. The VI-B and V–B group of transition metals have M_2AC bulk modulus similar to an equivalent MC (binary carbides).
2. The IV-B group of transition metals has a bulk modulus that is much smaller than that of MC (binary carbides) [44,73].

Furthermore, The compressibility of lattice parameters c with a is affected by the M and A atoms of the M_2AC phase [52]. **Table 6** provides a summary of the estimated shear (G), Poisson's ratio (ν), average compressibility β , Young's modulus (Y) and bulk (B). The variation between bulk moduli and shear moduli is relatively minor. The B was higher compared with G, indicating that G is the constraint for the stability of such materials. In addition, the MAX phases are brittle (ductile) if the percentage of B per G was lower

Table 6

The shear modulus (G) in Gpa, bulk modulus (B) in GPa, modulus of elastic (E) in Gpa, Compressibility (β), Vickers hardness (H_V) in GPa and Poisson ratio (ν) for the Zr_2AC MAX phase.

	B_V	B_R	B	G_V	G_R	G	B/G	β	E	ν	H	Ref				
Zr_2AlC	154.35	153.94	154.15	144.54	143.63	144.08	0.93	0.0065	329.57	0.143	6.4 ± 0.1	^a a [38]				
			131.6			99.5			238.4			0.1981	^a [74]			
			150										^a [39]			
Zr_2InC	148.86	148.84	125	125.78	120.78	93	0.202	0.0067	224	0.175	5.9	** [29]				
			148.85			123.28			289.83			0.2056	^a f [41]			
			130.9									0.2157	^a a [38]			
													** [43]			
													^a g/f [46]			
Zr_2TiC	148.53	148.34	113	136.75	136.33	99	0.72	0.0067	239	0.208	7.1	^a h [46]				
			137			93			226			0.220	^a [44]			
			148.44			136.54			313.50			0.148	^a [47]			
			135			92			226			0.220	^a a [38]			
			135			93			226			0.220	^a h [49]			
Zr_2SiC	152.76	148.63	115	94.31	63.67	80	0.52	0.0066	195	0.218	7.1	^a b [49]				
			114.8			80			195			0.218	^a a [38]			
			150.70			78.99			201.73			0.277	^a a [38]			
			173										^a [39]			
			150			97			239			0.234	^a f [41]			
Zr_2GeC	159	159	159	97	95	96	1.41	0.0066	240	0.24	7.1	[50]				
			151.53			99.34			84.06			91.70	0.61	228.74	0.247	^a a [38]
			147.8			71.9			76.2			74.0	0.61	190.4	0.286	^a [51]
			148.1			113.80			106.98			110.40	0.70	268.33	0.215	^a a [38]
			157.63			106.98			106.98			110.40	0.61	228.74	0.247	** [38]
Zr_2SnC	157.63	156.60	147.3	157.11	113.80	103.8	0.70	0.0063	252.1	0.215	7.1	^a [52]				
			157.12			110.40			268.33			0.215	^a a [68]			
			151.75			106.88			259.68			0.214	^a b [68]			
													3.5 ± 0.4	**c [54]		
														^a a [38]		
Zr_2PbC	148.23	148.10	148.17	118.21	106.32	112.26	0.75	0.0067	268.90	0.197	13.02	^a a [38]				
			116.25			78.12			191.47			0.23	^a e,f [55]			
			116.3			74.1			183.4			0.237	^a e,f [16]			
Zr_2PC	189.61	186.93	188.27	143.60	129.97	136.80	0.72	0.0053	330.36	0.207	7.8	^a a [38]				
			186										^a [39]			
													^a f [41]			
Zr_2AsC	156.24	154.41	155.32	80.40	13.63	47.20	0.30	0.0064	128.13	0.362	7.8	^a a [38]				
			166.90			135.05			130.97			133.01	0.80	315.20	0.184	^a a [38]
			163													^a [39]
Zr_2SC	186.65	187.22	186.94	126.18	130.43	128.31	0.7	0.0060	313.25	0.2207	6.8	^a b [56]				
			179.05			120.05			115.43						^a f [59]	
			182.23			121.22			115.55						^a h [59]	
			163									114		0.216	^a e,f [60]	
			166									116	0.7	282	0.217	^a f [41]
Zr_2SeC	154	154	154	100	0.65	100	0.65	0.0060	247	0.23	14.85 mac	^a e,f [61]				
															17.79 mic	
															18.10 mac	^a [63]
			150			108	0.720		262	0.209	21.02 mic					

^a Theoretical **experimental.

than 1.75. These materials exhibit brittle behavior [68]. Fig. 9 shows the change of the MAX phases B with A element depending on the electron density of the p orbital.

Table 6 shows the calculated ν , G, B, E, β , and H_V for the Zr_2AC MAX phase. From Table 6, the calculated mechanical properties, including the bulk modulus (B), shear modulus, and modulus of elastic (E), are analyzed in this review in order to obtain the differences in properties regarding the Zr_2AC MAX phases. When the A element such as Pb, Al, Si, Ge, Se, S, As, In, Sn, Tl, and P, it can mechanical properties change with constant transition metal (Zr). Furthermore, it found that the bulk modulus ranges were (113 GPa for Zr_2AlC –188.27 GPa for Zr_2PC), (47.2 GPa Zr_2AsC - 144.8 GPa Zr_2AlC), modulus of elastic (E) (128.13 GPa for Zr_2AsC -329.57 GPa for Zr_2AlC), thus other properties can be compared successfully.

A, FP-LAPW (full-potential linearized augmented plane-wave method); b, PP-PW (plane-wave pseudopotential); c, XRD (X-Ray Diffraction); d, NPD (Neutron Powder Diffraction); e, PBE (Perdew-Burke Ernzerhof formalism); f, GGA (energy functional used is the generalized gradient approximation); g, PW91 (Perdew-Wang's exchange-correlation function); h, LDA/CAPZ the localized density approximation for the Ceperly-Alder and Perdew-Zunger exchange-correlation function; T is represented TEM.

3.3.1. Mechanical properties of Zr_2AC MAX phase

The elasticity parameters allow researchers to consider that the Zr_2AC MAX phases are mechanically stable, except for the Zr_2PbC MAX phase is considered as brittle materials. From the studies of literature, the results revealed that Zr_2AC 's bulk modulus and shear modulus rise as p electrons of (A) elements travel rightwards in to the periodic table of Zr_2AC . Electronic structure study also explains

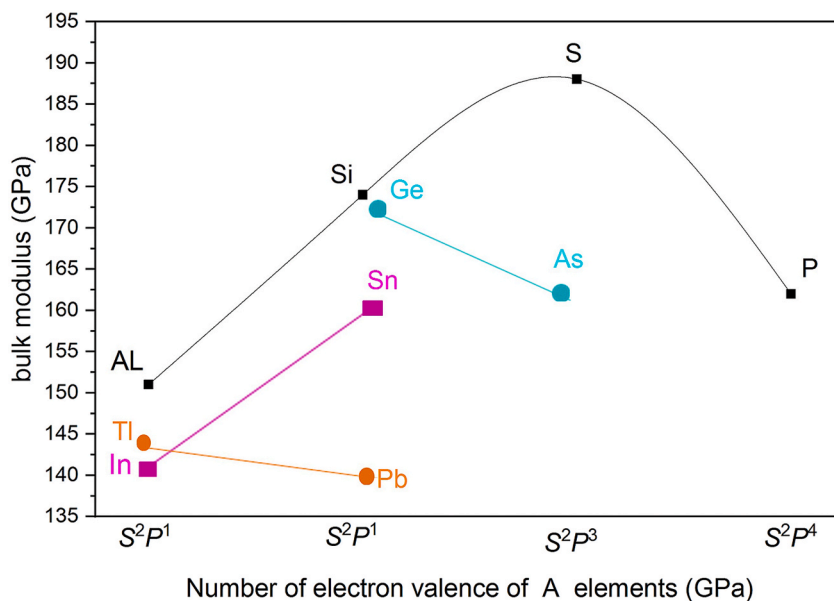


Fig. 9. The change of the MAX phases bulk modulus with A element depending on the electron density of the p orbital [38].

elastic stiffness trends as valence electron occupation near Zr_2AC 's to the EF. They show that bulk moduli greatly rise due to additional valence electrons in $Zr d-Ap$ states up to the $s2p3$ column [38,39,41]. Kanoun et al. (2010) indicated that these Zr_2AC (where A is Ti, In, Ti, Si, As, Sn, S, Pb, Ge P) MAX phase have a strong shear plane anisotropy. The shear modulus G_{VRH} limits the stability as $B_{VRH} > G_{VRH}$. They show that bulk moduli considerably rise due to additional valence electrons in $Zr d-A p$ states up to the $s2p3$ column. The brittleness and ductility are connected with a G_{VRH}/B_{VRH} ratio with a value of 0.57. Thus, the estimated G_{VRH}/B_{VRH} values for the Zr_2AC imply that Zr_2GeC as well as Zr_2SiC somewhat further ductile compared with other MAX phases. Furthermore, the Poisson ratio (ν) for covalent and metallic materials are 0.1 and 0.33 respectively while in Zr_2AC , ν values range of (0.10–0.36), showing a significant metallic with an ionic contribution to intra-atomic bonding. G_{VRH}/B_{VRH} values likewise support the Zr_2AC 's mixed ionic-covalent bonding range between 0.30 and 0.94. The Zr_2PC MAX phase exhibits a higher bulk modulus than Zr_2AC compounds, while Zr_2AlC , Zr_2TiC , and Zr_2PC exhibit the maximum G_{VRH} . The unit cell volumes and B of these MAX phases, are strongly correlated [38]. The above finding is consistent with the study done by Kang (2013). Kang (2013) shows that the Zr-A bond strength indicates the B of Zr_2AC (where A is P, S, Al, Si) MAX phases. Also, the bulk modulus rises depending on A element moving through the periodic table in a direction of $Al \rightarrow P$ for Zr_2AC (where A is P, S, Al, Si) MAX phases according to a progressive A-Zr enhancement (strengthening) [39]. In addition, Nasir et al. (2014), found that the B of Zr_2AC (where A is P, S, Al, Si) MAX phases increase with pressure and decrease with temperature, following the volume trend. The C–Zr bond is the hardest in the Zr_2AC phases. Nonetheless, the Zr–C bonds are shorter compared with the Zr-A bonds; thus, knowing the usual combination of hardness and bond length, researchers can suggest them to be harder. Also, the Zr_2AlC , Zr_2SiC , Zr_2PC , and Zr_2SC have estimated Vickers hardness values of 5.9, 7.1, 7.8, and 6.8 GPa. Again, when the A elements travel on the periodic table to the right side, theoretical hardness increases obviously. After that, a slight reduction in sulfur (Zr_2SC MAX phase) occurs in this case. It is noted that the bond hardness is highest with the smallest volume of the bond, and according to H_V , the Zr_2AlC is slightly easier to machine and soft than the other 3 MAX phases [41].

3.3.2. Mechanical properties of Zr_2AlC MAX phase

Lapauw et al. (2016) determined that the Zr_2AlC ceramic containing 28 vol% ZrC was subjected to a Vickers hardness test using a 30 N load. The resulting hardness value obtained was 6.4 ± 0.1 Gpa [29].

3.4. Mechanical properties of Zr_2SnC MAX phase

The Zr_2SnC MAX phase has excellent machinability; no lubrication or cooling system is required to machine it. It can machine using a hacksaw, milling machine, or lathe [54,67,68]. Additionally, Zr_2SnC has a great compressibility on the a-axis compared to the c-axis [68,75].

Barsoum et al. (1997) measured the hardness of the Zr_2SnC MAX phase under a load of 1 kg to be 3.5 ± 0.4 Gpa [54]. El-Raghy et al. (2000) fabricated a fully dense single-phase of Zr_2SnC (92 ± 94 vol%). The Vickers hardness, as well as Young's modulus, were 178 GPa and 3.9 ± 0.3 GPa, respectively, which is low by about 50% compared with equivalent binary carbides. Another hand, it shows the weakness of the M – Sn bonds compared with the M – C bonds and highly considered sensitivity to the composition and purity of the MAX phase. Although, most M_2AC phases, including M_2SnC phases, have comparable Vickers hardness values [67]. Furthermore, Bouhemadou (2008) calculated the linear relationship of the elastic stiffness with the pressure as well as shear and bulk moduli,

Poisson's ratio, and Young's moduli for ideal polycrystalline of the Zr_2SnC . In another study, Kanoun et al. (2008) calculated the bulk modulus values of these ternary carbides that are expected to be around 69% of those of the comparable binary carbides MC, a value close to $2/3$. Also, the $M_{n+1}AC_n$ bulk moduli are close to $n+1/n+2$ of the binary carbides for $n = 1$ and 2 . The present research is not investigating whether B (MAX phase bulk modulus) $M_{n+1}AC_n = n+1/n+2$ BMC (bulk modulus binary carbide) is due to chance or deeper physics [49]. In different studies, Kanoun et al. (2009) found that Zr_2SnC 's bulk, shear, and Young's modulus are minimal compared to other nanolaminate systems, and its compressibility (β) was 0.00636 (1/GPa) [68]. Consequently, Zr_2SnC is soft material that agrees with Barsoum et al. (1997) and El-Raghy et al. (2000) results [54,67,68]. The Zr_2SnC is somewhat anisotropic in compression and shear stress. Also, the elastic anisotropy is low in these MAX phases. However, the Zr_2SnC MAX phase is mechanically stable, and the shear, as well as bulk modulus results, indicate hard materials with high G or B [68].

3.4.1. Mechanical properties of Zr_2InC MAX phase

Many researchers have argued that the elasticity of the Zr_2InC is anisotropy, mechanically stable as well as brittle materials. The Zr_2InC phase compresses more along the c -axis than the a -axis, it is further incompressible across the a - and b -axes [43,44,46,52,65].

Manoun et al. (2004) fabricated Zr_2InC bulk polycrystalline. The hexagonal MAX phases have no peaks in the XRD spectra, even at 52 GPa. Consequently, this structure remains stable, comparable to the remaining MAX phases. The bulk modulus is 127 ± 5 GPa with a pressure variation of 4.25 ± 0.3 , which matches their *ab initio* estimates of 130.9 GPa. As expecting, the Zr_2InC has a lower bulk modulus than other types of M_3AX_2 phases. One obvious explanation is that the X-M bond is shorter and more powerful than the A-M. Therefore, the 211 MAX phase includes a greater portion of the "soft" M-A bonds compared to the 312 MAX phase. At 195 GPa, ZrC's 0 K (zero kelvin) is bigger than the one determined herein. The MAX phase formations resemble binary carbide rock salt structures [43]. In a different study, high-pressure effects on lattice parameters from 0 to 50 GPa were studied by Medkour et al. (2008), who found that c -axis contractions were larger compared with a -axis contractions. The measured value of bulk modulus is 117 GPa. Also, they found that the measured B from the elastic constants is quite close to the value that determined by the equation of state EOS fitting [44]. Bouhemadou (2008) also reported that the elasticity Zr_2InC is compressed more in the c -axis compared with the a -axis under pressure (0–20 GPa). The M–In (where M is Zr, Hf, Sc, Ti, V, and Ta) bond is more deformable compared with the C-M bond due to its increased compressibility along the c -axis. Furthermore, the B rise depending on the number of M valence electrons in M_2InC (where M is Zr, Hf, Sc, Ti, V, and Ta) MAX phase. Finally, the bulk moduli of Zr_2InC ($VEC = 4$) exhibit a substantial decrease compared to its binary carbide counterparts [52]. Otherwise, He et al. (2009) compared between the bulk modulus of M_2InC and M_2TiC (where M is Hf, Ti, and Zr), the Zr_2InC show the smallest B value among them theoretically. This demonstrated that B is also affected by A element [45]. Furthermore, Yang et al., (2013) indicated that the experimental evidence coincided with that the a -axis is more rigid than the c -axis below 37.5 GPa (GGA). However, ultra-incompressibility along the c axis is always between 70 and 400 GPa due to the delay of the Core-valence charge transfer. In addition, the fast displacement of the zirconium atom in the c -axis direction is attributed to this abnormal behavior since the percentage of c per a is restricted beyond 400 GPa (the Zr atom shift suspends along the c -axis). Also under pressure, the quick displacement of the zirconium atom in the c -axis direction has demonstrated similar change patterns to the percentage of c per a . The Zr–In bond densities and Zr with In atoms' pressure responses may also explain this phenomenon. The axial bulk moduli support the c -axis ultra-incompressibility. Therefore, this ultra-incompressibility has never been observed in MAX phases; the theoretical predictions are eagerly anticipated. The Zr_2InC 's structural instability and elastic softening from 70 to 160 to 700–850 GPa indicated structural transformation. Furthermore, Poisson's ratio showed that pressure increases ionicity in interatomic bonding. Also, the Zr_2InC is elastic isotropic, and pressure rapidly increases anisotropy. Thus, various characteristics have been obtained from isotropic to anisotropic conversion. The Zr_2InC is brittle at room temperature and minimizes with pressure, as in B/G and B/C₄₄ [46]. Recently, Sultana et al. (2018) gave a comprehensive review on individual crystal elastic constants as well as phonon dispersion curves of the Zr_2InC MAX phase, which supported mechanical and dynamical stability. The computed single crystal elastic constants C_{ij} along with polycrystalline elastic constants, rise according to the atomic number of M (where M is Zr, Hf, Ta) as in the M_2InC MAX phase. Furthermore, the Pugh and Poisson's ratios showed the Zr_2InC MAX phase brittleness due to strong directional covalent bonds and ionic contribution. Moreover, the ν of the Zr_2InC MAX phase is 0.20, indicating a combination of ionic with covalent bonding. The Cauchy pressure (C₁₂–C₄₄) (–28.5) displays a negative value reflecting that covalent bonding dominates in the Zr_2InC MAX phase. The MAX phases with low Vickers hardness such as Zr_2InC (1.05 GPa) are soft and easy to machine. However, the measured Vickers hardness value is in good agreement with elastic moduli, PDOS, and charge density mapping (CDM) [47]. Another study by Li et al., (2022) found that the sequence of anisotropy was $Zr_2InN > Zr_2InC$. The M_2InX phases match literature data in structural and elastic constants. Shear modulus is a superior hardness measure than the bulk modulus of the Zr_2InC phase, which is more incompressible across the a - and b -axes [65].

3.4.2. Mechanical properties of the Zr_2PbC MAX phase

Several studies have revealed that the Zr_2PbC MAX phase has a superior ability to machine. A manual hacksaw, milling machine, and lathe with ordinary tool bits can machine without lubrication or a cooling system. The Zr_2PbC MAX phase is mechanically stable [16,66]. El-Raghy et al., (2000) fabricated a fully dense single-phase of Zr_2PbC (92 ± 94 vol%) MAX phase. The Zr_2PbC Vickers hardness value is 3.2 ± 0.5 GPa [75]. Compared to most M_2AC phases, such as M_2SnC , this value agrees with their range for Vickers hardness [67]. In contrast, Qian et al., (2012) calculated Zr_2PbC 's G, which is 67 GPa, the lowest among MAX phases, because of the weak Pb–Zr bond [66]. In addition, a study by Khatun et al., (2020) showed that the Zr_2PbC is mechanically stable due to elastic characteristics, while at high pressure, it becomes unstable. The pressure decreases lattice constants and unit cell volume approximately linearly while increasing the hexagonal ratio gradually. Thus, a parameter drops quicker than the c parameter. Therefore, the c -axis compressibility is lower than the a -axis. The Zr_2PbC is brittle and elastically anisotropic, and the brittleness increases with

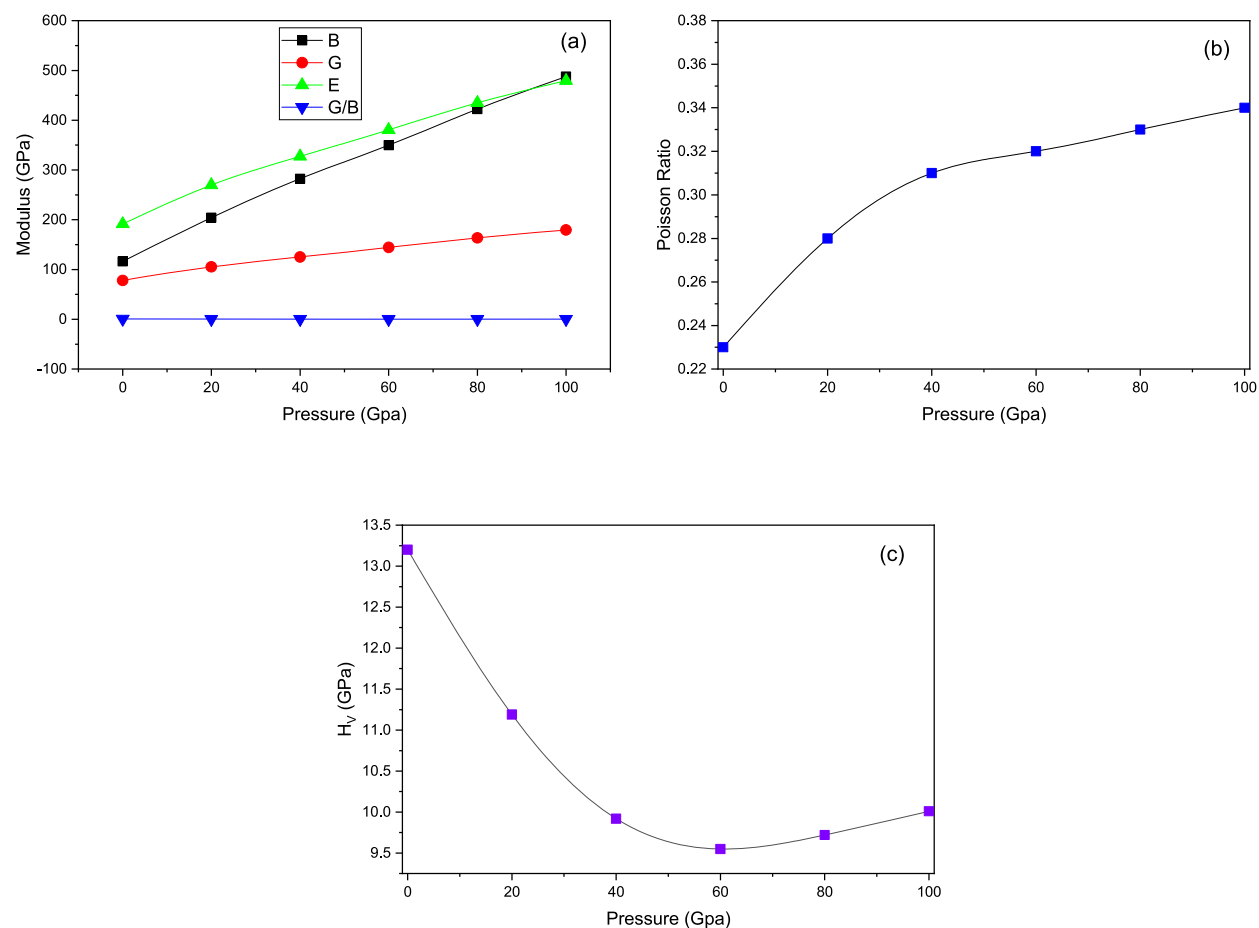


Fig. 10. Pressure(p) change effect (0–100) GPa on (a) the B, G, G/B, and E of Zr₂PbC (b) ν Zr₂PbC and (c) H_v of Zr₂PbC [55]. Poisson Ratio H_v (GPa).

pressure. The elastic constants satisfy Born's mechanical stability criterion and exhibit a monotonous growth of the five independent elastic constants C_{ij} (0–100) GPa. They have high directional covalent bonding because of their reduced Poisson ratios. Furthermore, pressure increases the B, G, and E in Zr₂PbC as illustrated in Fig. 10(a and b) and Table 7. Furthermore, the G/B ratios drop with pressure, hence Zr₂PbC brittleness can decrease progressively. The Zr₂PbC is hard based on Vickers's hardness. The study of Zr₂PbC's, B, G, H_v, and Y indicates increasing in the hardness of Zr₂PbC under pressure. Fig. 10(c) shows the pressure-dependent Vickers hardness (H_v) of the Zr₂PbC compound [55]. The research studied by ALrebbi et al., (2021) also found that the M₂PbC MAX phases exhibit inherent and mechanical stability at zero and under pressure along with a small elastic anisotropy due to stiffness constants. The investigation of the bulk modulus and tensile modulus remark to the exceptional hardness of the Zr₂PbC. In addition, the elastic constants such as C11 along with C33 were increased with pressure faster than other constants. The B > G indicates that the G is a stability-restriction factor [16].

3.4.3. Mechanical properties of the Zr₂SC MAX phase

Bouhemadou (2008) estimated the static finite strain technique and the elastic constants. He calculated the B, G, B/G, E, and Poisson ratio (ν) for the Zr₂SC MAX phase as displayed in Table 7 [56]. Kulkarni et al., (2008) also studied the Zr₂SC MAX phase using 46 GPa pressure at ambient temperature and found no phase transformation caused by this pressure. Both axes compress similarly to a maximum of 15 GPa; after that, the c-axis compresses considerably. The isothermal bulk modulus was $K_T = 186$ (4) GPa with a pressure derivative of 4.0. However, the compressibility was practically isotropic compared to the other 211 MAX. Table 8 illustrates pressure-dependent lattice parameters and unit cell volume [57]. However, Fu et al., (2009) evaluated the isothermal compressibility along with the elastic anisotropy coefficient of Zr₂SC individual crystals at pressures between 0 and 50 GPa. When pressure increases, Zr₂SC compressibility drops, while its anisotropy factor, c-axis as well as in-plane bulk moduli increase. Finally, the results of this study are explained in terms of lattice vibration anharmonicity, and atomic bonds across the a-axis are weaker compared with the c-axis [58].

Furthermore, Feng et al., (2010) found that the Zr₂SC MAX phase is best stable with the pressure range of (0–100) GPa, according to elastic constants change with pressure. The Zr₂SC MAX phase is brittle based on the bulk-shear modulus ratio. Also, the Zr₂SC's brittleness mechanism derives from the massive Zr atom filling the internal parameter Z_m [59]. In addition, according to Opeka et al.,

Table 7Shows the theoretical study of the Variation of the G, B/G, E, ν , B and H_V under P (0–100) GPa of Zr_2PbC [55].

P (GPa)	G	B	G/B	ν	E	H_V
0	78.12	116.25	0.67	0.23	191.47	13.2
20	105.38	204.29	0.52	0.28	269.76	11.19
40	125.29	282.5	0.44	0.31	327.46	9.92
60	144.38	349.91	0.40	0.32	380.77	9.55
80	163.71	422.39	0.38	0.33	434.94	9.72
100	179.39	487.75	0.37	0.34	479.40	10.01

Table 8

The experimental study of the Pressure-dependent lattice constants with unit cell volume [57].

P (GPa)	a (Å) (± 0.002)	c (Å) (± 0.03)	Vol (Å ³) (± 0.2)	a/a_0	c/c_0	v/v_0
0	3.406	12.14	122.0	1	1	1
2.91	3.396	12.08	120.6	0.9967	0.9954	0.9889
5.48	3.379	12.05	119.1	0.9918	0.9925	0.9764
10.94	3.347	11.94	115.8	0.9825	0.9834	0.9494
14.47	3.331	11.88	114.2	0.9778	0.9792	0.9363
18.21	3.315	11.83	112.5	0.9728	0.9745	0.9224
22.54	3.305	11.73	111.0	0.9701	0.9668	0.9100
24.68	3.293	11.69	109.8	0.9666	0.9634	0.9003
28.8	3.281	11.64	108.5	0.9631	0.9592	0.8897
31.02	3.269	11.60	107.3	0.9594	0.9558	0.8799
35.41	3.251	11.55	105.7	0.9541	0.9517	0.8663
39.31	3.236	11.51	104.3	0.9498	0.9480	0.8553
40.94	3.233	11.49	104.0	0.9489	0.9464	0.8523
44.89	3.220	11.43	102.6	0.9450	0.9417	0.8410
46.46	3.212	11.42	102.0	0.9427	0.9405	0.8360

(2011), the Zr_2SC MAX phase was an easy machine. Flexural strength up to 800 °C is approximately 250 MPa. Also, the plastic deformation occurred at range of (room temperature (RT) –2066 °C) in a load–deflection curves. The sample deflection during fracture was temperature-dependent, reaching a minimum of 1510 °C [76]. Research findings by Cui et al., (2013) also point towards reported that the Zr_2SC MAX phase is brittle because a smaller internal position of the M atom promotes Peierls stress (0.89 Gpa). On the other hand, compared to binary compounds, ternary compounds achieve higher optimum tensile strengths.

Furthermore, the structural breakdown of the M_2SC MAX phase is caused by the rupture of the poor covalent S-M bond under tensile stress. However, electronic instabilities under finite shear deformations cause plasticity in these MAX phases. The S-M bond under tensile tension determines M_2SC 's layered structural stability. It should be noted that this structure exhibits a lower resistance to shear deformation compared to tensile stress. The ideal shear strength of the M_2SC MAX phase is limited or lowered by the electronic instabilities (breakage of M – S covalent bonds), which in turn lead to elastic instability.

Additionally, the low B/G ratios along with negative Cauchy pressure (C12 – C44), indicate natural brittleness in M_2SC ceramics. They propose that M_2SC brittleness comes from bigger dislocation movement in a glide plane, which can be compressed via higher Peierls stress, which is released by the new layered structure of M_2SC ceramics. Finally, the tensile strength is 35 Gpa, and the shear strength is 24 Gpa [60].

3.4.4. Mechanical properties of the Zr_2SeC MAX phase

Stiffness parameters demonstrate the mechanical stability that exists in the Zr_2SeC MAX phase [61,63]. Ali and Qureshi (2021) indicated that the Zr_2SeC MAX phase exhibits lower stiffness, elastic moduli, and hardness properties than the Zr_2SC MAX phase. Based on bond lengths, DOS, as well as CDM results, explain the parameter reduction. The direction of the elastic moduli as well as anisotropy indices, shows that the Zr_2SeC MAX phase appears more anisotropic than the Zr_2SC MAX phase [61]. Akhter et al. (2022) also verified the Zr_2SeC mechanical stability as determined by the stiffness constants within a specific pressure range. Furthermore, the pressure affects elastic constants, elastic moduli, as well as hardness characteristics, with Zr_2SeC obtaining a lower pressure effect in these values than Hf_2SeC . Mechanical behavior characteristics rise with increasing pressure. The Zr_2SeC MAX phase is elastically anisotropic and brittle. However, up to 25 GPa, it becomes less brittle. At 5 and 10 GPa pressure, the Zr_2SeC MAX phase is ductile [63].

3.4.5. Mechanical properties of the Zr_2TiC MAX phase

Warner et al. (2006) measured B of the Zr_2TiC MAX phase, which is 120 GPa. The B of the M_2AC MAX phase is reduced in a direction (Al → Ga → Ti) for the same M, where M is Hf, Zr, and Ti. Also, the reduction of B between the M_2AlC and M_2GaC MAX phases was quite minor. However, the B drop is high from M_2AlC → M_2TiC , with a 25% maximum percentage. On the other hand, the Zr_2TiC MAX phase belongs to the second group, which is B considerably smaller compared with the equivalent part of binary carbide [48]. Bouhemadou (2009) also estimated the elastic constants G, B ν , and E for the ideal polycrystalline of the Zr_2TiC MAX phase as aggregating state [49].

3.4.6. Mechanical properties of the Zr_2GeC MAX phase

Bouhemadou (2009) reported that the B of the ternary carbides with a second transition metal rises as the following sequences $Zr_2GeC < Nb_2GeC < Mo_2GeC$. Moreover, the shear modulus C_{44} is (directly connected to hardness) and is highest whenever 8.41–8.50 is a range of the valence electron concentration (VEC). The bond energy of the C-M, as well as Ge-M bonds, rises along with the valence electron concentration (VEC) (average number of valence electrons/atoms), which increases bulk modulus [51].

3.4.7. Mechanical properties of the Zr_2SiC MAX phase

Ghebouli et al., (2015) found that the M_2SiC (where M is Cr, Hf, Nb, V, W, Mo, Ti, Ta, and Zr) each series of C44s saturates at 8.5 VEC. The distortion rises with VEC and reduces with the k_c/k_a factor (the proportion among the linear compressibility coefficients across the c -as well as a -axis used for calculating elastic anisotropy), excluding the series $Cr \rightarrow V \rightarrow Ti$, where it is smaller at 8.5 VEC (it follows a parabolic pattern). However, the shear plus elastic moduli peaks were at 8.5 VEC. Also, VEC raises distortion and bulk modulus. The M_2SiC MAX phase possesses significant anisotropy for shear planes (1010) and stronger compressibility in a axis compared with the c axis, but the W_2SiC MAX phase is excepted [50].

3.5. Thermal characteristics

The thermal characteristics of MAX phases taking the Debye temperature (θ_D) in to account are among the more crucial factors that affect the behavior of the MAX phase [38]. The Debye temperature of solid materials correlates with several physical parameters, including thermal expansion, thermal conductivity, melting temperature, specific heat, lattice vibration, and more [52]. It connects two important factors: superconductors' electron-phonon coupling factor and superconducting transition temperature. Furthermore, the energy needed to generate metal vacancies is linked to Debye temperature. The energy needed to generate metal vacancies is linked to Debye temperature. Debye temperature can be computed in numerous techniques. Anderson's technique, which depends on the average elastic (sound) wave velocity, is logical as well as straightforward [70].

Table 9 shows the thermal characteristics. From Table 9, the thermal characteristics were analyzed in order to show the differences in properties for the Zr_2AC MAX phase. When the A element such as Se, Si, P, Al, S, As, In, Ge, Sn, Tl and Pb, the thermal properties can change with constant transition metal (Zr). In addition, the thermal characteristics, including transverse, longitudinal, average sound

Table 9

Shows the determined transverse, longitudinal, average sound velocity (ν_t, ν_l , and ν_m in m/s) and density (ρ in g/cm^3), the minimum thermal conductivity K_{min} ($W m^{-1} K^{-1}$) and the debye temperatures (θ_D in K) for the Zr_2AC MAX phase.

	ρ	ν_l	ν_t	ν_m	θ_D	TCE ppm/K	α (K^{-1})	K_{min}	Ref
Zr_2AlC	5.286	5220	8093	5730	658.76				^a a [38]
Zr_2InC	7,10								**c [42]
	7.103	4166	6640	4587	520.60				^a a [38] ^b f/g [46] ^a h [46]
Zr_2TiC	9.117	3870	6020	4249	481.52				^a a [38]
	9.36 8.92	5253	3145	3480	398				^a h [49]
		4989	2993	3311	372				^a b [49]
Zr_2SiC	5.536	3777	6800	4207	490.32				^a a [38]
Zr_2GeC	6.541	3744	6461	4155	481.81				^a a [38]
	6.86	5998	3286	3664	432				^a [51]
Zr_2SnC	7.281	3893	6465	4306	490.64				^a a [38]
	7.75	6111	3683	4073	472				^a a [52]
	3.831	6357	4236		482.75				^a a [68]
	3.893	6464	4305		490.64				^a b [68]
	7.16						0.004		^a c [54]
	6.98								**c [54]
	7.16						8.3 ± 0.2	0.0035	^a c [67]
6.9								**c [67]	
Zr_2PbC	9.036	3524	5741	3890	438.45				^a a [38]
	9.2					8.2 ± 0.2	0.0144		^a c [67]
	9.1								**c [67]
	8.2								**c [67]
	9.037	2919	4920	3137	350.0				^a e,f [16]
Zr_2PC	8.870	2967	4984	3285	368.36				^a e,f [55]
Zr_2AsC	6.026	4764	7842	5264	628.40				^a a [38]
Zr_2SC	6.600	2669	5747	3006	348.56				^a a [38]
Zr_2SeC	5.711	4826	7761	5319	622.73				^a a [38]
	6.37	7494	4486	4964	603				^a b [56] ** [76]
Zr_2TeC						8.8			
	5.74	4459.03	7416.58	4931.78	409.62	3.88		1.3 1.06	^a e,f [61] ^a f [63]

^a Theoretical, ** experimental.

velocity (ν_t, ν_l , and ν_m in m/s) and density (r in g/cm^3), the minimum thermal conductivity K_{\min} ($\text{W m}^{-1} \text{K}^{-1}$) and the Debye temperatures (θ_D in K) for the Zr_2AC MAX phase as seen in Table 9. The density ranges from light MAX phase 3.831 (r in g/cm^3) for Zr_2SnC to heavy MAX phase 9.117 for Zr_2TiC , while the Debye temperatures (θ_D) range from 679 K for Zr_2SeC to 350.0 K to Zr_2PbC ; thus other properties can be compared in the same way.

A, FP-LAPW (full-potential linearized augmented plane-wave method); b, PP-PW (plane-wave pseudopotential); c, XRD (X-Ray Diffraction); d, NPD (Neutron Powder Diffraction); e, PBE (Perdew-Burke Ernzerhof formalism); f, GGA (energy functional used is the generalized gradient approximation); g, PW91 (Perdew-Wang's exchange-correlation function); h, LDA/CAPZ the localized density approximation for the Ceperly-Alder and Perdew-Zunger exchange-correlation function. The T is represented TEM.

3.4.1. Thermal properties of the Zr_2AC MAX phase

Nasir et al., (2014) claimed that the B of Zr_2AC (where A is S, Si, Al, and P) MAX phases rise with pressure at a given temperature while reducing with the temperature at a given pressure. Furthermore, the specific heat of Zr_2AC was greatly affected by ion interactions at low temperatures, while at elevated temperatures, a harmonic influence on specific heat is restrained all phases' Debye temperatures (θ_D) for Zr_2AC decrease nonlinearly with increasing temperature as well as the pressure dependence on the θ_D , which is a nonlinear increasing spontaneously. The change in θ_D with pressure and temperature demonstrates that the frequency of thermal vibration of atomic in these ternary nanolaminates can, in fact, change with these two variables. Particularly at low temperatures, the specific heat C_V of Zr_2AC is highly affected by the interactions between Zr_2AC ions. The influence of differing M-A bonds on C_V is negligible, as evidenced by the small changes in C_V (specific heat with constant volume V) between phases. The somewhat higher C_P (specific heat with constant pressure P) values for Zr_2AC can be explained by the following formula ($C_P - C_V = \alpha V^2 (T) BV T$) where α_V , V, T, and B denote, the thermal expansion coefficient of volume, volume, absolute temperature, and bulk modulus, respectively. The C_V approaches a constant value at high temperatures, but C_P gradually rises with temperature. The volume thermal expansion coefficient of Zr_2AC is found to rise sharply at low temperatures, approach a linear rise at high temperatures, and then become relatively moderate in its rate. Finally, at a constant temperature, the coefficient of expansion falls off sharply when the pressure (P) increases. Also, Zr_2AlC 's thermal expansion coefficient is determined to decrease marginally quicker than that of the other phases [41].

3.5.2. Thermal properties of the Zr_2SnC MAX phase

The Zr_2SnC MAX phase exhibited metallic behavior depending on the temperature coefficient of resistivity (α) [54,67]. Barsoum et al. (1997) produced a single-phase, fully dense of the Zr_2SnC MAX phase. They found that the coefficient of the temperature of resistivity (α) of the Zr_2SnC MAX phase was 0.004 K^{-1} , showing a metallic-like temperature dependency of the resistivity [54]. In contrast, El-Raghy et al., (2000) fabricated a fully dense single-phase of the Zr_2SnC ($92 \pm 94 \text{ vol}\%$) MAX phase. They found that the temperature coefficient of resistivity (α) of the Zr_2SnC MAX phase is 0.0035 K^{-1} , which is lower than the value obtained by Barsoum et al. (1997) [54,67]. The thermal coefficient of expansion (TCEs) is $8.3 \pm 0.2 \text{ ppm/K}$. The ternaries' TCE matches the stoichiometric binaries' (20–33%). As a result, the M – C bonds in ternary compounds are similar (comparable) to those in stoichiometric binary compounds (counterparts). Although, some ternary M – C bonds may be considerably stronger [67]. In addition, Bouhemadou (2008) calculated Zr_2SnC 's Debye temperature using the average sound velocity as illustrated in Table 9 [52]. The research study by Kanoun et al. (2009) also predicted that the Zr_2SnC MAX phase owns a somewhat elevated θ_D value revealing that has a rather stiff crystal structure or lattice, so the thermal conductivity to be excellent. The gradual decrease in mean sound velocity of the Ti – Zr – Nb – Hf series also explains that Debye temperatures tend to decrease in the same order [55]. Another hand Kanoun et al. (2010) demonstrated that the high Debye temperature implies a higher associated thermal conductivity [38].

3.5.3. Thermal properties of the Zr_2InC MAX phase

Using phonon dispersion patterns, Sultana et al. (2018) evaluate the thermodynamic parameters of M_2InC (where M is Ta, Zr, and Hf) MAX phases. The good agreement with the properties of M atomic species is discovered for the free energy, enthalpy, entropy, specific heat capacity, and Debye temperature [47]. Furthermore, Li et al. (2022) found that the Zr_2InC 's lattice thermal conductivity at room temperature is $23.59 \text{ W m}^{-1} \text{K}^{-1}$. Thus, at ordinary temperatures, the Zr_2InC MAX phase can be used as potential materials for thermal conduction. As temperature rises, thermal conductivity (k_{ph}) rapidly drops and, at some point, stabilizes. The $\text{Ti}_2\text{InC} > \text{Zr}_2\text{InC} > \text{Ti}_2\text{InN} > \text{Zr}_2\text{InN}$ is the order of k_{ph} from 300 K to 1300 K. Unlike $\text{Ln}_2\text{Zr}_2\text{O}_7$, M_2InX phases cannot form high-temperature thermal barrier coatings [65].

3.5.4. Thermal properties of the Zr_2pbC MAX phase

El-Raghy et al., (2000) fabricated the Zr_2pbC with purity of ($92 \pm 94 \text{ vol}\%$). The temperature coefficient of resistivity (α) of the Zr_2pbC MAX phase is 0.0144 K^{-1} , showing a metallic-like temperature dependency of the resistivity. The thermal coefficient of expansion (TCEs) is $8.2 \pm 0.2 \text{ ppm/K}$. The ternaries' TCE matches the stoichiometric binaries' (20–33%). The C-M bond in ternary compounds is similar to stoichiometric binary compounds. Some ternary M – C bonds may be considerably stronger [67]. In a different study, Khatun et al., (2020) observed that melting temperature, Debye temperature θ_D , and minimum thermal conductivity (K_{\min}) rise with pressure, as indicated in Table 10 [55]. The K_{\min} increases with pressure due to the average sound velocity increasing with pressure spontaneously. Furthermore, Alrebdy et al., (2021) reported that the Zr_2pbC (Zr, Hf, and Ti) MAX phase has a comparatively large value of θ_D , indicating a rigid lattice and higher thermal conductivity. The gradual decrease in the average speeds of sound in the $\text{Ti} \rightarrow \text{Zr} \rightarrow \text{Hf}$ sequences supports the tendency to lower θ_D in a similar order in the M_2pbC MAX phases [16].

Table 10

The theoretical calculations of the longitudinal sound velocity (v_l), transverse sound velocity (v_t), evaluated density ρ , average sound velocity v_m and θ_D of Zr_2PbC under pressure & K_{min} ($Wm^{-1}K^{-1}$) [55].

Pressure (GPa)	$\rho(kg/m^3)$	v_t (m/s)	v_l (m/s)	v_m (m/s)	$\theta_D(K)$	K_{min}
0	8870	2967.70	4984.87	3285.47	368.36	0.14
20	10080	3233.32	5848.59	3602.51	421.49	0.16
40	10900	3390.35	6422.10	3790.23	455.25	0.18
60	11670	3517.37	6817.59	3938.23	483.84	0.20
80	12200	3663.18	7246.65	4106.72	512.14	0.21
100	12790	3745.10	7538.99	4202.90	532.40	0.23

3.5.5. Thermal properties of the Zr_2SC MAX phase

The θ_D of the M_2SC MAX phase is estimated from the average sound velocity as reported in Table 9 by Bouhemadou et al., (2008) [56]. Fu et al., (2009) also measured the thermal expansion of the Zr_2SC MAX phase single crystals under pressure of 0–50 GPa. The debye temperature of the Zr_2SC MAX phase drops significantly with increasing temperature. The pressure increases longitudinal as well as transverse wave velocities and it decreases compressibility. Anharmonicity of lattice vibrations is used to interpret the results [58]. While Opeka et al., (2011) synthesized the Zr_2SC MAX phase at 1750 °C with high properties such as excellent laminated structure, thermal stability to up 2100 °C, thermal shock resistance, and easily machineable. Furthermore, within a 25 to 2000 °C temperature range, the material exhibited a thermal expansion coefficient of 8.8×10^{-6} per °C. At temperature of 100 °C, the thermal conductivity (κ) was measured to be 38 W/m.K, and at 1100 °C, it was approximately 30 W/m.K. The specific heat ranged from 0.4 to 0.5 kJ/kg °C. The Load–deflection curves showed plastic deformation from 25 to 2066 °C. While at 1510 °C, specimen deflection at fracture was the lowest [76].

3.5.6. Thermal properties of the Zr_2SeC MAX phase

Ali and Qureshi (2021) indicated that the temperature and pressure-dependent characteristics vary as expected. Furthermore, the factors of the Zr_2SeC 's MAX phase, such as θ_D , T_m , K_{min} , and TEC are lower than those of the Zr_2SC MAX phase, and its C_v reaching the classical θ_D limit at a lower temperature than the Zr_2SC 's MAX phase. Thus, the factors of the Zr_2SeC 's MAX phase, such as θ_D , K_{min} , TEC, and T_m values, are comparable to those of $Y_4Al_2O_9$ [61]. Chen et al. (2021) also demonstrated that the Zr_2SeC 's MAX phase electron thermal conductivity contribution triggered at elevated temperatures balances for the decreasing tendency to thermal conductivity contribution. These findings show that A-site components tune the MAX phase's physical characteristics while the M-A atom interactions determine the MAX phases' physical and chemical characteristics. Thus, Zr–Se atom interactions explain the heat conductive behavior. The thermal conductivity (κ) of the Zr_2SC MAX phases and Zr_2SeC are 21.10 W/m-K and 18.30 W/m-K, respectively. Otherwise, the thermal conductivity of the Zr_2SeC MAX phase decreased when the temperature rose from RT to 600 K while it remained constant (18.5 W/m-K) with the Zr_2SC MAX phase at a temperature range of (RT–500) °K. Furthermore, the phonon transport dominates the normal thermal behavior (75.2% for Zr_2SeC , 80.6% for Zr_2SC). The Zr_2SeC MAX phase has a larger electronic contribution than the Zr_2SC MAX phase, especially at high temperatures due to the Se atoms big size and lower electronegativity weakening the Zr–Se bond. Another reason, the Zr_2SeC 's MAX phase weaker Zr–Se bond releases additional 4 *d* electrons at the EF in atoms of Zr comparable to the Zr_2SC MAX phase, and these delocalized electrons may be generated at high temperatures [62]. In addition, Akhter et al. (2022) studied parameters of the Zr_2SeC MAX phase at a pressure range of 0–25 Gpa relevant to thermal properties suitability for high-temperature applications. The parameters of the Zr_2SeC MAX phase at a pressure range of 0–25 Gpa are relevant to thermal properties and vary with pressure. As shown by its melting point, debye temperature, and minimal thermal conductivity, the Zr_2SeC MAX phase may be employed as a coating material for thermal barriers TBC materials at elevated temperatures [63]. Furthermore, Wang et al. (2022) compared between thermal properties of Hf_2SeC , Hf_2SC , Zr_2SeC , and Zr_2SC . S-MAX phases (Hf_2SC and Zr_2SC) achieved lower CTEs than the Se-MAX phases because of the strong M-A bond. The thermal expansion of these four chalcogenide MAX phases was isotropic, matching the approximation adjustment of anisotropy with C_{11}/C_{33} [72].

3.5.7. Thermal properties of the Zr_2TiC MAX phase

Bouhemadou (2009) calculated the debye temperature of the Zr_2TiC MAX phase from the average sound velocity. Table 10 illustrates the calculated density (ρ in g/cm^3), the longitudinal, transverse, average sound velocity (v_l , v_t , and v_m in m/s), the debye temperatures (θ_D in K), and the minimum thermal conductivity K_{min} ($W m^{-1} K^{-1}$) for the Zr_2AC MAX phase [49].

3.5.8. Thermal properties of the Zr_2SiC MAX phase

Ghebouli et al., (2015) calculated the minimum thermal conductivity and the debye temperature of the M_2SiC MAX phase, and the highest value was observed at a VEC of approximately 8.5 [50].

3.6. Optical properties

Studying solids' optical characteristics of the MAX phase is interesting. Compared to structural and electrical characteristics, the MAX phases' optical properties have been few discussed in the literature. The complex dielectric function is a crucial property that requests further investigation, as it represents the basic feature of a material's linear reaction to the wave of electromagnetic [66].

3.6.1. Optical properties of the Zr_2AC MAX phase

Kanoun et al. (2010) indicated that the difference in spectral features of the optical characteristic of the Zr_2AC MAX phase (where A is As, Ge, Tl, In, Si, Sn, P, Pb, S, Ti) to the band structures have different dispersions as a result permitted to optical transfer to occur between varying states. Furthermore, the changes in the optical property dispersion, moving from left to right by substituting Al with As, Ge, P, S, Si, In, Sn, Pb, and Tl through the periodic table, is a significant study. Otherwise, the determined optical characteristics was utilized to identify the optical absorption and the optical spectrum. These compounds' band structures are different, which affects optical transitions and peak positions. The maximum reflectivity at a range of (12–14) eV arises from transitions of inter-band. The lowest reflectance at 22–25 eV verifies a collective plasma resonance around 35.0 eV. The Zr_2AC MAX phase exhibits a rapidly rising in reflectivity [64]. In another study, Nasir et al. (2014) found that three Zr_2AC MAX phases (where A is P, Si, and Al) are suitable coating materials for lowering solar heating except for the Zr_2SC MAX phase owing to its reflectivity spectra being greatly influenced [41]. Furthermore, Qureshi et al. (2022) investigated the dielectric as well as photoconductive behavior of M_2AC (where M is Hf, Zr, Cr, and A is Ga, Al) terminated surface (0001), the optical characteristics of the more stable (0001) surfaces are required. From a thin-film standpoint, the M(C)- terminated surface and A-terminated surface possess appropriate absorbing characteristics. The M_2AC are dielectric coating possibilities due to positive static dielectric constant value, $\epsilon_1(0)$. Additionally, the M_2AC MAX phase coatings are electrically conductive after absorbing the energy of photons in the UV, IR, and visible regions [69].

3.6.2. Optical properties of the Zr_2SnC MAX phase

Kanoun et al. (2009) estimated the optical characteristics by calculating the optical absorption and optical spectrum. These curves slightly differ due to band structure changes in M_2SnC (Hf, Nb, Ti, and Zr) MAX phases, which affect the optical transitions and the peak positions [68]. While, Hadi et al. (2022), found that the dielectric function $\epsilon_1(0)$ is a non-zero value; as a result, the high existence of carriers of free charge in that metallic system was obtained. Furthermore, the Zr_2SnC MAX phase is anisotropic up to 7 eV concerning photon energy across both polarizations. The Zr_2SnC MAX phase is high reflects light at low frequencies, indicating high conductivity and low absorption power. The Zr_2SnC MAX phase has an average reflectivity of more than 40% in the visible light range for the two polarizations, making it an appropriate coating material for decreasing solar heating. The Zr_2SnC MAX phases have anisotropic optical properties, and it is not having an optical conductivity above 17 eV from the photon energy. The Zr-c bonds were expected to be highly localized (restricted) while the weaker Zr–Sn bonds were less localized and much more scattered out. The charge transfer in the Zr_2SnC MAX phase is modest due to the Bader charge analysis [77].

3.6.3. Optical properties of the Zr_2InC MAX phase

Sultana et al. (2018) found that the visible reflectivity curves are continuously above 45% and maximum at 91%, around 8.94 eV within the Zr_2InC MAX phase. Thus, the compounds are interesting candidates for visible and ultraviolet optoelectronic device applications and as coating materials to avoid solar heating [47].

3.6.4. Optical properties of the Zr_2PbC MAX phase

Qian et al., (2012) noted that the imaginary component of the Zr_2PbC MAX phase's dielectric function is comparable to Ti_2PbC 's. The Zr_2PbC 's imaginary portion is roughly (one eV) due to transitions within the Zr-d bands, and the peak of approximately (3 eV) coincides with the transition through (Pb/C p - Zr d) states. The Zr_2PbC MAX phase exhibits a plasma frequency peak at (13.5 eV). When the incident light frequency is higher than the plasma frequency, the material becomes transparent [66]. Khatun et al., (2020) also indicated that due to the metallic nature of the Zr_2PbC MAX phase, optical characteristics such as absorption and conductivity originate at zero photon energy. They found that increasing the operating pressure is related to spontaneously increasing the photoconductivity and absorption. Furthermore, the reflectance spectra of the visible light suggest that the Zr_2PbC MAX phase can reduce solar heating as a coating material [55].

3.6.5. Optical properties of the Zr_2SeC MAX phase

Ali and Qureshi (2021) found that Zr_2SeC 's photoconductivity curves and dielectric coefficient match the band structure data, indicating metallicity. Additionally, the optical characteristics of the Zr_2SeC MAX phase suggest its application as a solar heating shield. The Zr_2SeC optical properties are anisotropic such as their electrical conductivity and mechanical properties [61]. This study agrees with Akhter et al. (2022) publisher. Furthermore, according to their high reflectivity within the low energy state, the produced Zr_2SeC MAX phase can be reflectors of the solar heat [63].

3.7. Nuclear properties

Zirconium-based materials are explored for the nuclear industry owing to their modest thermal neutron cross-section area. The fuel cladding materials of the next-generation reactor of light water (Gen-III + LWR) must be cost-effective and endure harsh work conditions including thermal and mechanical stresses, significant neutron irradiation dosage, and extremely corrosive or oxidative surroundings. MAX phases with excellent outstanding properties, may be used for fuel cladding in bulk or as coatings in nuclear application [29,78]. The MAX phases with high-purity are needed for nuclear fuel coating due to their radiation resistance, mechanical properties, plus coolant suitability (anti-oxidation and anti-corrosion) [30]. The M and A elements were selected based on the neutron cross-section and synthesizability of the M_2AlC as well as Zr_2AC ternary MAX phases. Despite failing the second selection criterion, Mo, As, and Sb were selected due to their similar qualities to their old MAX phase neighbours in the periodic table [79].

3.7.1. Nuclear properties of the Zr_2AlC MAX phase

Horlait et al. (2016) suggested using the Zr_2AlC MAX phase for the application of the nuclear due to its excellent neutron transparency and potential resistance of irradiation. Also, the Zr_2AlC MAX phase, like other Al-based MAX phases, has suitable high-temperature oxidation resistance, making it an effective protective coating material for modified accident tolerant fuel assembly grids [79]. Lapauw et al. (2016) also suggested that the utilization of the MAX phase has been proposed as a potential safeguard against the high-temperature steam surroundings that may arise in Gen-III + LWRs in the event of a loss of coolant (LOCA) incident that the Zr_2AlC MAX phase is a significant MAX phase that exhibits the ability to be superior to the zircaloy clads that are currently utilized in commercial applications [29]. More recently, Qarra et al. (2019) investigated the highest dose of irradiating 3.5 displacements/atom for the (66% Zr_2AlC MAX phase + 33 wt% ZrC) at RT-600 °C. The High-temperature irradiated Zr_2AlC remained crystalline. However, the (0001) basal planes had more dislocations and stacking defects. Like other MAX phase materials, the irradiation material showed temperature-dependent micro-cracking. The Zr_2AlC resists radiation damage poorly at low temperatures. The micro-cracks show that continuous operation temperatures above 300 °C, are appropriate for structural applications. This phase's low neutron absorption cross-section and irradiation endurance are useful for nuclear applications under these conditions. This phase's Zr neutron transparency improves reactor neutronics and fuel economy. Aluminum also generates an oxide layer of protection that enhances its resistance to oxidation caused by high-temperature steam. For nuclear applications, especially reactor core materials, irradiation resistance is critical. Thus, many MAX phases have undergone irradiation resistance testing. Irradiated MAX phases' tolerances are particularly sensitive to elements and accurate stoichiometry, according to this research [34]. On the other hand, Tunca et al. (2017) showed that the synthesized Zr–Al–C-based MAX phases including Zr_3AlC_2 and Zr_2AlC are promising for nuclear application. Zr–Al–C MAX phases ideal fuel cladding materials due to their small neutrons cross-sectional area. Post-Fukushima, the nuclear industry is developing accident-tolerant fuel (ATF) clad compounds that exceed zircaloy clad in light water reactors. These materials must survive steam oxidation at elevated temperatures, water corrosion, and radiation with good endurance [80]. Tang et al. (2017) also investigated the Zr–C–Al system's coatings. The coating focused on the possible manufacturing of Zr_2AlC and Zr_3AlC_2 MAX phases over Zircaloy-4 clad substrates as protection against accidental steam with elevated temperature oxidation. It was feasible to produce a nanoscale element multilayer structure with Zr, C, and Al layers in different stacking sequences that matched the crystal structures of the Zr_2AlC and Zr_3AlC_2 MAX phases. However, no MAX phases were formed after argon annealing at 600–1200 °C. Three different Zr/Al ratios were deposited on polished Zircaloy-4 substrates, matching the structures of crystals of, $Zr_2Al_4C_5$, Zr_2AlC , and $Zr_3Al_3C_5$. Furthermore, three coats oxidized slower than untreated Zircaloy-4 oxidizing over 700 °C for 250 min in steam. The coatings with the highest content of Al ($Zr_2Al_4C_5$, and $Zr_3Al_3C_5$) were the best oxidation-resistant. However, due to the thermal expansion imbalance between substrate and coatings, these two coatings had poor adhesion to Zircaloy-4 substrates and; spallation & extensive cracks during oxidation. All coatings were oxidized at 800 °C and 1000 °C [81]. However, Chen et al. (2018) indicated that some MAX phases, particularly Al-containing, have better oxidation and resistance corrosion at high temperatures and easy machinability due to their nanolayered structure. Additionally, MAX phases are appropriate for accident-tolerant fuel clads in light water reactor, which experience thermal and mechanical stresses, intense neutron irradiation, and oxidation. 70 MAX phase types have been developed experimentally and despite of that due to Zr's narrow neutron cross-section, Zr–Al–C MAX ceramics like Zr_3AlC_2 and Zr_2AlC are promising fuel cladding coatings [40]. In a different study by Lapauw et al. (2019) the MAX phase-based ceramics exposure to in an oxygen-poor liquid lead-bismuth eutectic (LBE) system under static and fast-flowing conditions. Despite the lack of a repeated scale of oxide on the exposed MAX phase ceramics, the majority of MAX phases exposed to static and oxygen-poor (LBE) ($C^\circ < 2.2 \times 10^{-10}$ mass %) at 500 °C for 1000 h showed excellent chemical suitability for a heavy of liquid metal. Only Zr-rich MAX phases showed localized LBE chemical reactions. Additionally, Pb/Bi-containing solid solutions of (Zr_2 (Bi, Pb, Al) C) appear from localized LBE reaction with Zr-rich MAX phases. LBE also entered the ceramic bulk due to the dissolution of parasitic intermetallic compounds and the chemical reaction of static liquid LBE with Zr-based MAX phases. However, purity is critically required for the MAX phase that is used in the systems of cooled nuclear of HLM. The erosion resistance of MAX phase ceramics was increased by 1000 h of exposure to oxygen-poor ($C^\circ \approx 5 \times 10^{-9}$ mass %) high-speed-flowing ($v \approx 8$ m/s) liquid LBE at 500 °C. Although, this section's main findings are that oxidation was a major corrosion mechanism despite moderate oxygen concentration and no damage of erosion to the exposed of the MAX phase [82].

Agine, Tunca et al. (2019) considered the product of both Zr_3AlC_2 and Zr_2AlC MAX phases as promising fuel cladding material candidates. Phase purity is critical for nuclear MAX phase synthesis to prevent in-service material breakdown caused by the coefficient of thermal expansion (CTE) gap among gradient phases and/or anisotropic irradiation swelling. The MAX phase ceramic intrinsic characteristics require high phase purity. The Zr–Al–C MAX phase production with high purity demonstrated a real challenge. The highest obtain purity was 67% Zr_2AlC +33% of ZrCx) weight ratio. Earlier search developed (Zr,Ti) $_2$ AlC as well as (Zr,Ti) $_3$ AlC $_2$ solid solution MAX phases to improve Zr_2AlC MAX phase resistance oxidation. Unfortunately, these solid solutions from the MAX phases had many secondary phases [30]. Finally, Tunca et al. (2020) exposed to the Zr_2AlC ceramics comprising (67% Zr_2AlC + 33% ZrC) wt. to oxygen-poor ($C^\circ \leq 2.2 \times 10^{-10}$ mass%), after 1000 h of static liquid LBE at 500 °C, as the following:

1. Al outward diffusion between Zr_2AlC grains towards the grain borders (GB) and Bi/Pb penetration into the grains generated a novel solid solution in situ, Zr_2 (Al, Bi, Pb)C MAX. Bi/Pb atoms initially infiltrated basal planes, potentially across stacking faults (SFs) or defect-rich regions in MAX phase grains, and subsequently dispersed throughout Zr_2AlC grains.
2. The blend of (Pb, Al, Bi) A-layers of a solid solution of the Zr_2 (Al, Pb, Bi)C MAX phase had out-of-plane order with sequences of big and small concentrations of Al.
3. Following LBE exposure/annealing for 1000 h at 500 °C, the non-LBE impacted Zr_2AlC MAX phase formed a super-lattice structure.

The research offers two avenues: (1) Employing ZrC-based diffusion obstacles on the Zr₂AlC MAX phase decreases Zr₂AlC and LBE interactions and thus enhances the service life of the substrate of fuel clad; (2) Zr₂(Bi, Pb, Al)C solid solution, exhibits more stability along with less neutron absorption compared with Zr₂AlC MAX phase, may be an appropriate replacement for fuel clads of Gen-IV LFR. This solid solution's coats need additional work to increase phase purity and realize their full potential [83].

3.8. Corrosion and oxidation resistance of the Zr₂AlC MAX phase

3.8.1. The corrosion and oxidation resistance of the Zr₂AlC MAX phase

Kovalev and coworkers (2017) found that the Zr₂AlC MAX phase represents the type of 211 MAX phase and it is presumed to be highly resistant to oxidation temperature [84]. Chen et al. (2018) also showed that nanolayered structures, particularly those comprising aluminium, possess a blend of properties that are typically associated with both ceramics and metals. These properties include easy machinability and exceptional oxidation and corrosion resistance at high temperatures [40]. This finding is consistent with the study by Lapauw et al. (2016) that the 211-stoichiometric MAX phase demonstrates superior resistance to oxidation because it contains a high amount of aluminium, which enables the formation of a protective layer of Al₂O₃ oxide. The volume expansion connected to the process of oxidation allows the Al₂O₃ to 'heal' cracks and restore the material strength significantly [29].

3.8.2. The corrosion and oxidation resistance of the Zr₂InC MAX phase

Gupta and co-workers (2006) synthesized the Zr₂InC MAX phase sample containing 95 vol% single phases, ZrC_x ~2 vol%, and excess In to 3.5 vol%. The oxide layers produced at 400 °C that is not withstand oxidation. The chemical reaction yields are In₂O₃ plus transition metal ions with its oxides. Furthermore, the ZrO₂ in Zr-base MAX-phase may be amorphous, although the primary substance is nanocrystalline. Also, the grain growth kinetics of the In₂O₃ hinder by transition metal oxide. However, at elevated temperatures, catastrophic oxidation followed incubation. The In situations inner oxygen diffusion caused oxidizing. Moreover, at moderate temperatures of 400–700 °C, the ternary carbides rapidly oxidize to create transition metal oxides and even the In₂O₃ MAX phase. Even oxidation-resistant M₂InC phases can be penetrated by oxygen. In fact, the rotating bearings, connections of electrical spinning, and other vital technology can use this low-wear as well as friction materials [85].

3.8.3. The Zr₂SC MAX phase

Opeka et al., (2011) showed that at temperatures beneath 500 °C, the Zr₂SC MAX phase can be applied in oxidation surroundings for long periods. For example, at 2150 °C and 23 s for arc heater investigation, the adherent and protection layer can be generated by the Zr₂SC MAX phase.

3.9. The self-healing property

The layering of products of oxidation along with ternary oxides may gain benefit through competing oxidation reactions. The Gibbs free energy of the oxide fabrication from M, A, and oxygen mixtures and it can be analyzed to discover advanced healing agents. For intense, SiO₂ with ZrO₂ form ZrSiO₄ (ternary oxide. Furthermore, basic properties restore depending on the healing agent's plus the substrate's adherence. The Stress-induced cracking, along with spallating, were unwanted outcomes of lattice orientation and thermal expansion coefficient (TEC) mismatch. Also, the TEC differences between MAX phase transition metal oxide can reduce adhesion and strength recovery. Depending on the explained parameters, the greatest crack-healing potential is MAX phases, those containing Ga, Si, and Al. The promising ternary oxide ZrSiO₄ MAX phase has a minimal thermal expansion rate as well as a Gibbs free energy of creating oxides among SiO₂ + ZrO₂. Nevertheless, Zr, as well as Si MAX phases, still needed to be produced. Investigations on the huge stable set of Al-containing compounds suggest self-healing materials are possible [86].

3.10. The self-healing property of the ZrAlC MAX phase

Lapauw et al. (2016) studied the self-healing ability of the MAX phase and proposed high-temperature selective oxidation for fracture or crack healing in Zr₂AlC. Other than ZrO₂, Al₂O₃ can arise in the form of an oxidation product, and the aluminium may enhance the hydrothermal stability of ZrO₂ scales [29]. Kovalev and coworkers (2017) also studied the Zr–Al–C system's phase development during SHS via time-resolved X-ray diffraction (TRXRD). They use two synthesis temperatures: a high of about 1730 °C and a low temperature (350–400 °C) at a rate of 250 K/min. They observed that an elevated temperature pulse starts the reaction that propagates ZrC's burning wave in SHS, and the final compound contains intermetallic zirconium phases. Otherhand, the bulk fire of the 2Zr–Al–C blend beneath situations of big heat removal throughout the chemical reaction among an (aluminum) melt as well as (zirconium) particles leads to the sequential creation of the Zr [Al] solid solution, ZrAlC_x phase, and the intermetallic compounds of the ZrAl₃, ZrAl₂, and Zr₂Al₃ phases owing to the small enthalpy of the chemical reactions between the aluminium and zirconium [84]. On the other hand, Tomoshige et al., (2019) produced the Zr₂SC MAX phase via SHS using a molar concentration of Zr:S: C = (2:1:1), the transition metal molybdenum was included in a molar concentration of Zr:Mo:S:C = 2-x:x:1:1 (x is (0–1.2)) to try to generate a solid solution of the MAX phases. The following results are obtained.

1. SHS process is readily manufactured of the Zr₂SC MAX phase with ZrC as well as Mo₂C byproducts.
2. A 20% molybdenum-zirconium solid solution was predicted.
3. The composite hardened mostly due to Mo₂C formation and little due to solid solution formation.

4. According to TEM, the Mo-added MAX phase had thin layers 10 nm broad.
5. The material characteristics of the Mo-added Zr₂SC MAX phase are significantly distinct from those of monolithic Zr₂SC, suggesting that it can be a potential material, especially in solid lubricity [87].

4. Conclusion

The $M_{n+1}AX_n$ are the general formal of the MAX phase; it became the Zr₂AC MAX phase when the transition metal is zirconium and n equals two. The $M_{n+1}AX_n$ layers are sandwiched between one-atom-thick metallic A-layers (pure element layers) in MAX phases. The Zr₂AC MAX phase belongs to a group of ternary carbide ceramics with layered structures that combine the desirable properties of both metals and ceramics. The chemical bonds of MAX phases are a blend of ionic, covalent, and metallic materials. Furthermore, the $M_{n+1}AX_n$ phases are receiving greater interest owing to their unique and occasionally abnormal characteristics, attributed to their layered structure and the tendency for basal dislocations to multiply and exhibit mobility under ambient conditions. In addition, the Zr₂AC MAX-phases exhibit numerous physical and chemical properties due to their chemical and structural characteristics. This review offers a comprehensive explanation of the properties of Zr₂AC MAX phases that have been the subject of theoretical or experimental research, as they are directly linked to the exceptional properties of MAX phase products and their applications. The Zr₂AC (A = P, Si, Se, Al, Sn, In, As, Pb, S, Tl, and Ge) MAX phases display properties such as structural, electronic, elastic, thermal, optical, and nuclear properties, as well as corrosion and oxidation resistance and self-healing properties. Compared with experimental work, the Zr₂AC lattice parameters a and c are deviation theoretically by 0.1–2% and 0.15–2.87%. Although the Zr₂AC MAX phases are metallic, their conductivity depends on the type of the Zr₂AC MAX phases (change of A element). The degree of p orbitals filling (A) elements determines the mechanical properties of Zr₂AC layered carbides. However, the MAX phases tend to be very stiff and isotropic regarding elastic properties. The Zr₂AC MAX phases exhibit hardness levels, ranging from 3.5 to 13.02 GPa, and high machinability with damage tolerance. The Zr₂AC MAX phases are also lightweight and resistant to thermal shock, oxidation, and corrosion. In addition, they behave as nonlinear elastic solids. At high temperatures, a transition from brittle to plastic behaviour occurs in the material, and its mechanical response is highly dependent on the rate of deformation. The Zr₂AC MAX phase possesses anisotropic optical, electrical, and mechanical characteristics.

Finally, this review thoroughly explains MAX phases while highlighting their recent progressive expansion and advancements. The investigation encompasses 211 Zr₂AC (A = P, Si, Se, Al, Sn, In, As, Pb, S, Tl, and Ge) MAX phases.

Declarations

Author contribution statement

All authors listed have significantly contributed to the development and the writing of this article.

Data availability statement

Data will be made available on request.

Additional information

No additional information is available for this paper.

Declaration of competing interest

The authors declare that they have no known competing financial interests or personal relationships that could have appeared to influence the work reported in this paper.

Acknowledgments

The English editing services provided by Curtin University's English Language Centre in Western Australia are acknowledged with gratitude by the researchers. The authors have received support from the Nanotechnology Society and the Environment Department at the University of Technology Iraq-Baghdad. The authors express their appreciation towards the anonymous reviewers and the editor for their valuable insights and comments. The authors express their gratitude towards the anonymous reviewers and the editor for their valuable insights and comments.

References

- [1] A.M.H. Abdulkadhim, *On The Stability of MAX Phase Thin Films*. PhD Diss, Aachen, Techn. Hochsch., Diss, 2011.
- [2] A. Abdulkadhim, M. to Baben, V. Schnabel, M. Hans, N. Thieme, C. Polzer, P. Polcik, J.M. Schneider, Crystallization kinetics of V2AlC, Thin Solid Films 520 (2012) 1930, <https://doi.org/10.1016/j.tsf.2011.09.037>. –1933.
- [3] M.A. Hadi, Superconducting phases in a remarkable class of metallic ceramics, J. Phys. Chem. Solid. 138 (2020), 109275, <https://doi.org/10.1016/j.jpcs.2019.109275>.

- [4] A. Azzouz-Rached, M.M. Haque Babu, H. Rached, T. Hadji, D. Rached, Prediction of a new Sn-based MAX phases for nuclear industry applications: DFT calculations, *Mater. Today Commun.* 27 (2021), 102233, <https://doi.org/10.1016/j.mtcomm.2021.102233>.
- [5] I. Ouadha, H. Rached, A. Azzouz-Rached, A. Reggad, D. Rached, Study of the structural, mechanical and thermodynamic properties of the new MAX phase compounds (Zr_{1-x}Ti_x)₃AlC₂, *Comput. Condens. Matter.* 23 (2020), e00468, <https://doi.org/10.1016/j.cocom.2020.e00468>.
- [6] K. Khalaf Al-Khazrajy, A.M.H. Al-Ghaban, M. Nabih Ali Hussain, The effect of aluminum concentration on the phase evolution of the ternary ceramics of (Ti-Al-C) system, *Eng. Technol. J.* 33 (2015) 973–984, <https://doi.org/10.30684/etj.33.4a.18>.
- [7] S. Aryal, R. Sakidja, M.W. Barsoum, W.Y. Ching, A genomic approach to the stability, elastic, and electronic properties of the MAX phases, *Phys. Status Solidi Basic Res.* 251 (2014) 1480–1497, <https://doi.org/10.1002/pssb.201451226>.
- [8] M.A. Rayhan, M.A. Ali, S.H. Naqib, A.K.M.A. Islam, First-principles study of Vickers hardness and thermodynamic properties of Ti₃SnC₂ polymorphs, *J. Sci. Res.* 7 (2015) 53–64, <https://doi.org/10.3329/jsr.v7i3.23182>.
- [9] M. Griseri, B. Tunca, S. Huang, M. Dahlqvist, J. Rosén, J. Lu, P.O.Å. Persson, L. Popescu, J. Vleugels, K. Lambrinou, Ta-based 413 and 211 MAX phase solid solutions with Hf and Nb, *J. Eur. Ceram. Soc.* 40 (2020) 1829–1838, <https://doi.org/10.1016/j.jeurceramsoc.2019.12.052>.
- [10] M.A. Ali, M.S. Ali, M.M. Uddin, Structural, elastic, electronic and optical properties of metastable MAX phase Ti₅SiC₄ compound, *Indian J. Pure Appl. Phys.* 54 (2016) 386–390.
- [11] G. Ying, C. Hu, L. Liu, C. Sun, D. Wen, J. Zhang, Y. Zheng, M. Wang, C. Zhang, X. Wang, C. Wang, Mechanical properties of phase-pure bulk Ta₄AlC₃ prepared by spark plasma sintering and subsequent heat treatment, *Process. Appl. Ceram.* 15 (2021) 211–218, <https://doi.org/10.2298/PAC2103211Y>.
- [12] N. Miao, J. Wang, Y. Gong, J. Wu, H. Niu, S. Wang, K. Li, A.R. Oganov, T. Tada, H. Hosono, Computational prediction of boron-based MAX phases and MXene derivatives, *Chem. Mater.* 32 (2020) 6947–6957, <https://doi.org/10.1021/acs.chemmater.0c02139>.
- [13] M.A. Ali, M.M. Hossain, A.K.M.A. Islam, S.H. Naqib, Recently Predicted Ternary Boride Hf₃PB₄: Insights into the Physical Properties of This Hardest Possible Boride MAX Phase, 2020, <https://doi.org/10.1016/j.jallcom.2020.158264>. ArXiv.
- [14] M.W. Qureshi, M.A. Ali, X. Ma, Screen the thermomechanical and optical properties of the new ductile 314 MAX phase boride Zr₃CdB₄: a DFT insight, *J. Alloys Compd.* 877 (2021), 160248, <https://doi.org/10.1016/j.jallcom.2021.160248>.
- [15] C. Hu, C.C. Lai, Q. Tao, J. Lu, J. Halim, L. Sun, J. Zhang, J. Yang, B. Anasori, J. Wang, Y. Sakka, L. Hultman, P. Eklund, J. Rosen, M.W. Barsoum, Mo₂Ga₂C: a new ternary nanolaminated carbide, *Chem. Commun.* (2015) 6560–6563, <https://doi.org/10.1039/c5cc00980d>.
- [16] T.A. Alrebdy, M.B. Kanoun, S. Goumri-Said, Physical properties investigations of ternary-layered carbides m2pbc (M = ti, zr and hf): first-principles calculations, *Crystals* 11 (2021), <https://doi.org/10.3390/cryst11121445>.
- [17] R.A. Majed, A.M. Haasan, R.F. Faleh, Corrosion behavior of V₂AlC and Cr₂AlC materials in acidic media, *Eng. Tech. J.* 33 (2015) 845–854, <https://doi.org/10.30684/etj.33.4A.8>.
- [18] A. Abdulkadhim, T. Takahashi, D. Music, F. Munnik, J.M. Schneider, MAX phase formation by intercalation upon annealing of TiC_x/Al (0.4 ≤ x ≤ 1) bilayer thin films, *Acta Mater.* 59 (2011) 6168–6175, <https://doi.org/10.1016/j.actamat.2011.06.029>.
- [19] A.A. Atiyah, A. Al-Ghaban, M.A.N. Al-Keshwan, Investigation of solid state reaction in the ternary Ti-Al-C, Cr-Al-C and V-Al-C systems A, *Eng. Tech. J.* 35 (2017) 764–771, [https://doi.org/10.1016/0040-6031\(85\)85934-7](https://doi.org/10.1016/0040-6031(85)85934-7).
- [20] M. Sokol, V. Natsu, S. Kota, M.W. Barsoum, On the chemical diversity of the MAX phases, *Trends Chem* 1 (2019) 210–223, <https://doi.org/10.1016/j.trechm.2019.02.016>.
- [21] Y. Rached, A.A. Ait Belkacem, D. Rached, H. Rached, M. Caid, M. Merabet, S. Benalia, L. Djoudi, I.E. Rabah, M. Rabah, The stability and electronic and thermal transport properties of new Ti-based MAX-phase compound Ta₂TiX (X: C or N), *Phys. Status Solidi Basic Res.* (2022), <https://doi.org/10.1002/pssb.202200195>.
- [22] S.I. Abdelsalam, A.M. Alsharif, Y. Abd Elmaboud, A.I. Abdellateef, Assorted kerosene-based nanofluid across a dual-zone vertical annulus with electroosmosis, *Heliyon* 9 (2023), e15916, <https://doi.org/10.1016/j.heliyon.2023.e15916>.
- [23] M.M. Bhatti, S.I. Abdelsalam, Scientific breakdown of a ferromagnetic nanofluid in hemodynamics: enhanced therapeutic approach, *Math. Model Nat. Phenom.* 17 (2022), <https://doi.org/10.1051/mmnp/2022045>.
- [24] H.B. Zhang, Y.C. Zhou, Y.W. Bao, M.S. Li, Improving the oxidation resistance of Ti₃SiC₂ by forming a Ti₃Si_{0.9}Al_{0.1}C₂ solid solution, *Acta Mater.* 52 (2004) 3631–3637, <https://doi.org/10.1016/j.actamat.2004.04.015>.
- [25] F.L. Meng, Y.C. Zhou, J.Y. Wang, Strengthening of Ti₂AlC by substituting Ti with V, *Scripta Mater.* 53 (2005) 1369–1372, <https://doi.org/10.1016/j.scriptamat.2005.08.030>.
- [26] M.W.B. c Y.L. Du a, b, Z.M. Sun a,*, H.Hashimoto a, A, Theoretical investigations on the elastic and thermodynamic properties of Ti₂AlC_{0.5}N_{0.5} solid solution, *Phys. Lett. Sect. A Gen. At. Solid State Phys.* 374 (2009) 78–82, <https://doi.org/10.1016/j.physleta.2009.10.023>.
- [27] W. Yu, V. Mauchamp, T. Cabioch, H. D. Magne, L. Gence, L. Piraux, V. Gauthier-Brunet, S. Dubois, Solid solution effects in the Ti₂Al(C_xN_y) MAX phases: synthesis, microstructure, electronic structure and transport properties, *Acta Mater.* 80 (2014) 421–434, <https://doi.org/10.1016/j.actamat.2014.07.064>.
- [28] S.T. Ahams, A. Shaari, R. Ahmed, M.C. Idris, N.F.A. Pattah, U. Teknologi, Ab-initio calculations of the structural and electronic properties of Zr₂AC, *Proc. Sci. Math* 1 (2020) 41–46.
- [29] T. Lapauw, K. Lambrinou, T. Cabioch, J. Halim, J. Lu, A. Pesach, O. Rivin, O. Ozeri, E.N. Caspi, L. Hultman, P. Eklund, J. Rosén, M.W. Barsoum, J. Vleugels, Synthesis of the new MAX phase Zr₂AlC, *J. Eur. Ceram. Soc.* 36 (2016) 1847–1853, <https://doi.org/10.1016/j.jeurceramsoc.2016.02.044>.
- [30] B. Tunca, T. Lapauw, R. Delville, D.R. Neuville, L. Hennet, D. Thiaudière, T. Ouisse, J. Hadermann, J. Vleugels, K. Lambrinou, Synthesis and characterization of double solid solution (Zr,Ti)₂(Al,Sn)₂C MAX phase ceramics, *Inorg. Chem.* 58 (2019) 6669–6683, <https://doi.org/10.1021/acs.inorgchem.9b00665>.
- [31] P. Sciences, Self-Healing Behaviour of Max Phase Ceramics Studied by Computer X-Ray Tomography. PhD Diss, The University of Manchester: The Faculty Of Engineering And Physical Sciences School of Materials, 2018.
- [32] S.H. Shah, P.D. Bristowe, Point defect formation in M₂AlC (M = Zr,Cr) MAX phases and their tendency to disorder and amorphize, *Sci. Rep.* 7 (2017), <https://doi.org/10.1038/s41598-017-10273-6>.
- [33] W.Y. Ching, Materials informatics using ab initio data: application to MAX phases, *Springer Mater. Sci.* 225 (2015) 187–212, https://doi.org/10.1007/978-3-319-23871-5_10.
- [34] H.H. Qarra, K.M. Knowles, M.E. Vickers, S. Akhmadaliev, K. Lambrinou, Heavy ion irradiation damage in Zr₂AlC MAX phase, *J. Nucl. Mater.* 523 (2019) 1–9, <https://doi.org/10.1016/j.jnucmat.2019.05.034>.
- [35] A. Abdulkadhim, M. to Baben, T. Takahashi, V. Schnabel, M. Hans, C. Polzer, P. Polcik, J.M. Schneider, Crystallization kinetics of amorphous Cr₂AlC thin films, *Surf. Coating. Technol.* 206 (2011) 599–603, <https://doi.org/10.1016/j.surfcoat.2011.06.003>.
- [36] M. Magnuson, M. Mattesini, Chemical bonding and electronic-structure in MAX phases as viewed by X-ray spectroscopy and density functional theory, *Thin Solid Films* 621 (2017) 108–130, <https://doi.org/10.1016/j.tsf.2016.11.005>.
- [37] M.B. Kanoun, S. Goumri-Said, M. Jaouen, Steric effect on the M site of nanolaminated compounds M₂SnC (M = Ti, Zr, Hf and Nb), *J. Phys. Condens. Matter* 21 (2009), <https://doi.org/10.1088/0953-8984/21/4/045404>.
- [38] M.B. Kanoun, S. Goumri-Said, A.H. Reshak, A.E. Merad, Electro-structural correlations, elastic and optical properties among the nanolaminated ternary carbides Zr₂AC, *Solid State Sci.* 12 (2010) 887–898, <https://doi.org/10.1016/j.solidstatesciences.2010.01.035>.
- [39] D.-B. Kang, Influence of different A elements on bonding and elastic properties of Zr₂AC (A = Al, Si, P, S): a theoretical investigation, *Bull. Kor. Chem. Soc.* 34 (2013), <https://doi.org/10.5012/bkcs.2013.34.2.609>.
- [40] L. Chen, M. Dahlqvist, T. Lapauw, B. Tunca, F. Wang, J. Lu, R. Meshkian, K. Lambrinou, B. Blanpain, J. Vleugels, J. Rosen, Theoretical prediction and synthesis of (Cr_{2/3}Zr_{1/3})₂AlC_{1-x}MAX phase, *J. Inorg. Chem.* 57 (2018) 6237–6244.
- [41] M.T. Nasir, M.A. Hadi, S.H. Naqib, F. Parvin, A.K.M.A. Islam, M. Roknuzzaman, M.S. Ali, Zirconium metal-based MAX phases Zr₂AC (A = Al, Si, P and S): a first-principles study, *Int. J. Mod. Phys. B* 28 (2014), <https://doi.org/10.1142/S0217979215500228>.
- [42] W. Jeitschko, H. Nowotny, F. Benesovsky, Die H-Phasen Ti₂InC, Zr₂InC, Hf₂InC und Ti₂GeC, *Monatsh. Chem.* 94 (1963) 1201–1205, <https://doi.org/10.1007/BF00905711>.

- [43] B. Manoun, S.K. Saxena, H.P. Liermann, R.P. Gulve, E. Huffman, M.W. Barsoum, G. Hug, C.S. Zha, Compression of Zr 2InC to 52 GPa, *Appl. Phys. Lett.* 85 (2004) 1514–1516, <https://doi.org/10.1063/1.1784516>.
- [44] Y. Medkour, A. Bouhemadou, A. Roumili, Structural and electronic properties of M2InC (M = Ti, Zr, and Hf), *Solid State Commun.* 148 (2008) 459–463, <https://doi.org/10.1016/j.ssc.2008.09.006>.
- [45] X. He, Y. Bai, Y. Li, C. Zhu, M. Li, Ab initio calculations for properties of MAX phases Ti2InC, Zr2InC, and Hf2InC, *Solid State Commun.* 149 (2009) 564–566, <https://doi.org/10.1016/j.ssc.2008.12.047>.
- [46] Z.J. Yang, L. Tang, A.M. Guo, X.L. Cheng, Z.H. Zhu, X.D. Yang, Origin of c-axis ultraincompressibility of Zr2InC above 70 GPa via first-principles, *J. Appl. Phys.* 114 (2013) 1–11, <https://doi.org/10.1063/1.4819174>.
- [47] F. Sultana, M.M. Uddin, M.A. Ali, M.M. Hossain, S.H. Naqib, A.K.M.A. Islam, First principles study of M2InC (M = Zr, Hf and Ta) MAX phases: the effect of M atomic species, *Results Phys.* 11 (2018) 869–876, <https://doi.org/10.1016/j.rinp.2018.10.044>.
- [48] J.A. Warner, S.K.R. Patil, S.V. Khare, K.C. Masiulaniec, Ab initio calculations for properties of MAX phases Ti 2 TiC, Zr 2 TiC, and Hf 2TiC, *Appl. Phys. Lett.* 88 (2006) 1–3, <https://doi.org/10.1063/1.2182009>.
- [49] A. Bouhemadou, Structural, electronic and elastic properties of Ti2TiC, Zr2TiC and Hf2TiC, *Cent. Eur. J. Phys.* 7 (2009) 753–761, <https://doi.org/10.2478/s11534-009-0022-z>.
- [50] B. Ghebouli, M.A. Ghebouli, M. Fatmi, L. Louail, T. Chihi, A. Bouhemadou, First-principles calculations of structural , electronic , elastic and thermal properties of phase M2SiC (M = Ti , V , Cr , Zr , Nb , Mo , Hf , Ta and W), *Trans. Nonferrous Metals Soc. China* 25 (2015) 915–925, [https://doi.org/10.1016/S1003-6326\(15\)63680-9](https://doi.org/10.1016/S1003-6326(15)63680-9).
- [51] A. Bouhemadou, Calculated Structural , Electronic and Elastic Properties of M 2 GeC (M = Ti , V , Cr , Zr , Nb , Mo , Hf , Ta and W), 2009, pp. 959–967, <https://doi.org/10.1007/s00339-009-5106-5>.
- [52] A. Bouhemadou, CALCULATED STRUCTURAL AND ELASTIC PROPERTIES OF M 2 InC (M = Sc , Ti , V , Zr , Nb , Hf , Ta), vol. 22, 2008, pp. 2063–2076.
- [53] T. Lapauw, B. Tunca, D. Potashnikov, A. Pesach, O. Ozeri, J. Vleugels, K. Lambrinou, The double solid solution (Zr, Nb)2(Al, Sn)C MAX phase: a steric stability approach, *Sci. Rep.* 8 (2018), <https://doi.org/10.1038/s41598-018-31271-2>.
- [54] M.W. Barsoum, G. Yaroshuk, S. Tyagi, Fabrication and characterization of M2SnC (M = Ti, Zr, Hf and Nb), *Scripta Mater.* 37 (1997) 1583–1591, [https://doi.org/10.1016/S1359-6462\(97\)00288-1](https://doi.org/10.1016/S1359-6462(97)00288-1).
- [55] R. Khatun, S. Sarkar, Structural , elastic , electronic , optical and thermodynamic properties of MAX phase compound Zr 2 PbC under pressure : DFT based investigation, *Comput. Condens. Matter.* 26 (2020), e00512, <https://doi.org/10.1016/j.cocom.2020.e00512>.
- [56] A. Bouhemadou, R. Khenata, Structural, electronic and elastic properties of M2SC (M = Ti, Zr, Hf) compounds, *Phys. Lett. Sect. A Gen. At. Solid State Phys.* 372 (2008) 6448–6452, <https://doi.org/10.1016/j.physleta.2008.08.066>.
- [57] S.R. Kulkarni, N.A. Phatak, S.K. Saxena, Y. Fei, J. Hu, High pressure structural behavior and synthesis of Zr2SC, *J. Phys. Condens. Matter* 20 (2008), <https://doi.org/10.1088/0953-8984/20/13/135211>.
- [58] H. Fu, J. Yang, Z. Zhao, P. Feng, W.F. Liu, T. Gao, Static compressibility, thermal expansion and elastic anisotropy of Zr2 SC single crystals, *Solid State Commun.* 149 (2009) 2110–2114, <https://doi.org/10.1016/j.ssc.2009.07.054>.
- [59] W. Feng, S. Cui, H. Hu, P. Feng, Z. Zheng, Y. Guo, Z. Gong, First-principles study on electronic structure and elastic properties of hexagonal Zr2Sc, *Phys. B Condens. Matter* 405 (2010) 4294–4298, <https://doi.org/10.1016/j.physb.2010.07.029>.
- [60] S. Cui, D. Wei, H. Hu, Z. Gong, Mechanical instability and ideal strengths of layered M2SC (M = Ti, Zr, and Hf) compounds, *J. Appl. Phys.* 113 (2013), <https://doi.org/10.1063/1.4791709>.
- [61] M.A. Ali, M.W. Qureshi, Newly synthesized MAX phase Zr2SeC: DFT insights into physical properties towards possible applications, *RSC Adv.* 11 (2021) 16892–16905, <https://doi.org/10.1039/d1ra02345d>.
- [62] K. Chen, X. Bai, X. Mu, P. Yan, N. Qiu, Y. Li, MAX P hase Zr 2 SeC and I ts thermal conduction behavior, *J. Eur. Ceram. Soc.* 41 (n.d.) 4429–4670 <https://doi.org/10.1016/j.jeurceramsoc.2021.03.013>.
- [63] M. Akhter, S. Ahasan, M.A. Ali, F. Parvin, Thermodynamic Properties of M 2 SeC (M = Hf , Zr) under High Pressure Elastic , Electronic , Optical , and Thermodynamic Properties of M 2 SeC (M = Hf , Zr) under High Pressure, 2023, 025154, <https://doi.org/10.1063/5.0136222>.
- [64] M.B. Kanoun, S. Goumri-Said, A.H. Reshak, A.E. Merad, Electro-structural correlations, elastic and optical properties among the nanolaminated ternary carbides Zr2AC, *Solid State Sci.* 12 (2010) 887–898, <https://doi.org/10.1016/j.solidstatesciences.2010.01.035>.
- [65] B. Li, Y. Duan, M. Peng, L. Shen, H. Qi, Anisotropic Elastic and Thermal Properties of M2InX (M = Ti, Zr and X = C, N) Phases, vol. 12, A First-Principles Calculation, 2022, <https://doi.org/10.3390/met12071111>. *Metals* (Basel).
- [66] X. Qian, N. Wang, Y. Li, Y. Zhou, H. Wu, Y. Li, X. He, First-principle studies of properties of ternary layered M 2PbC (M = Ti, Zr and Hf), *Comput. Mater. Sci.* 65 (2012) 377–382, <https://doi.org/10.1016/j.commatsci.2012.08.004>.
- [67] T. El-Raghy, S. Chakraborty, M.W. Barsoum, Synthesis and characterization of Hf2PbC, Zr2PbC and M2SnC (M = Ti, Hf, Nb or Zr), *J. Eur. Ceram. Soc.* 20 (2000) 2619–2625, [https://doi.org/10.1016/S0955-2219\(00\)00127-8](https://doi.org/10.1016/S0955-2219(00)00127-8).
- [68] M.B. Kanoun, S. Goumri-Said, A.H. Reshak, Theoretical study of mechanical, electronic, chemical bonding and optical properties of Ti2SnC, Zr2SnC, Hf2SnC and Nb2SnC, *Comput. Mater. Sci.* 47 (2009) 491–500, <https://doi.org/10.1016/j.commatsci.2009.09.015>.
- [69] M. Waqas, X. Ma, X. Zhang, G. Tang, Ab-initio Predictions of Phase Stability , Electronic Structure , and Optical Properties of (0001) -MAX Surfaces in M 2 AC (M = Cr , Zr , Hf ; A = Al , Ga), 2022.
- [70] S.T. Ahams, A. Shaari, N.F.A. Pattah, M. Buba, Structures , Electronic , and Transport Properties of M 2 PbC (M = Zr , V), *Int. J. Adv. Eng. Manag.* 4 (n.d.) 706–716. <https://doi.org/10.35629/5252-0404706716>.
- [71] S.J. Blundell, K.M. Blundell, *Concepts in Thermal Physics*, Oxford University Press on Demand, 2010.
- [72] X. Wang, K. Chen, E. Wu, Y. Zhang, H. Ding, N. Qiu, Y. Song, S. Du, Z. Chai, Q. Huang, Synthesis and thermal expansion of chalcogenide MAX phase Hf2SeC, *J. Eur. Ceram. Soc.* 42 (2022) 2084–2088, <https://doi.org/10.1016/j.jeurceramsoc.2021.12.062>.
- [73] D. Music, Z. Sun, R. Ahuja, J.M. Schneider, Coupling in nanolaminated ternary carbides studied by theoretical means: the influence of electronic potential approximations, *Phys. Rev. B Condens. Matter* 73 (2006) 1–5, <https://doi.org/10.1103/PhysRevB.73.134117>.
- [74] A. Bouhemadou, R. Khenata, M. Chegaar, Structural and elastic properties of Zr 2AlX and Ti 2AlX (X = C and N) under pressure effect, *Eur. Phys. J. B* 56 (2007) 209–215, <https://doi.org/10.1140/epjb/e2007-00115-6>.
- [75] A. Bouhemadou, Prediction study of structural and elastic properties under pressure effect of M2SnC (M=Ti, Zr, Nb, Hf), *Phys. B Condens. Matter* 403 (2008) 2707–2713, <https://doi.org/10.1016/j.physb.2008.02.014>.
- [76] M. Opeka, J. Zaykoski, I. Talmy, S. Causey, Synthesis and characterization of Zr2SC ceramics, *Mater. Sci. Eng.* 528 (2011) 1994, <https://doi.org/10.1016/j.msea.2010.10.084>. –2001.
- [77] M.A. Hadi, N. Kelaidis, P.P. Filippatos, S.R.G. Christopoulos, A. Chronos, S.H. Naqib, A.K.M.A. Islam, Optical response, lithiation and charge transfer in Sn-based 211 MAX phases with electron localization function, *J. Mater. Res. Technol.* 18 (2022) 2470–2479, <https://doi.org/10.1016/j.jmrt.2022.03.083>.
- [78] D. Hussein, K. Abbas, A. Abdulkadhim Al-Ghaban, Overview in technical synthesis and applications of Zr2AC (A= in, Sn, Pb, Al, S and Se) MAX phases: a brief review, *Eng. Technol. J.* 41 (2023) 1–15, <https://doi.org/10.30684/etj.2022.136391.1313>.
- [79] D. Horlait, S. Grasso, A. Chronos, W.E. Lee, Attempts to synthesise quaternary MAX phases (Zr, m) 2ALC and Zr2(ALA)C as a way to approach Zr2ALC, *Mater. Res. Lett.* 4 (2016) 137–144, <https://doi.org/10.1080/21663831.2016.1143053>.
- [80] B. Tunca, T. Lapauw, O.M. Karakulina, M. Batuk, T. Cabioch, J. Hadermann, R. Delville, K. Lambrinou, J. Vleugels, Synthesis of MAX phases in the Zr-Ti-Al-C system, *Inorg. Chem.* 56 (2017) 3489–3498, <https://doi.org/10.1021/acs.inorgchem.6b03057>.
- [81] C. Tang, M. Stueber, M. Steinbrueck, M. Grosse, S. Ulrich, H.J. Seifert, Evaluation of Magnetron Sputtered Protective Zr-Al-C Coatings for Accident Tolerant Zircaloy Claddings, 2017 Water React. Fuel Perform. Meet. Ramada Plaza Jeju • Jeju Island, Korea. September 10 (Sun) ~ 14 (Thu), 2017, Karlsruhe Institute of Technology, 2017, pp. 1–9. IAM-AWP, POB 3640, 76021 Karlsruhe, Germany chongchong.tang@kit.edu.

- [82] T. Lapauw, B. Tunca, J. Joris, A. Jianu, R. Fetzter, A. Weisenburger, J. Vleugels, K. Lambrinou, Interaction of Mn+1AXn phases with oxygen-poor, static and fast-flowing liquid lead-bismuth eutectic, *J. Nucl. Mater.* 520 (2019), <https://doi.org/10.1016/j.jnucmat.2019.04.010>.
- [83] B. Tunca, T. Lapauw, C. Callaert, J. Hadermann, R. Delville, E.N. Caspi, M. Dahlqvist, J. Rosén, A. Marshal, K.G. Pradeep, J.M. Schneider, J. Vleugels, K. Lambrinou, Compatibility of Zr2AlC MAX phase-based ceramics with oxygen-poor, static liquid lead–bismuth eutectic, *Corrosion Sci.* 171 (2020), <https://doi.org/10.1016/j.corsci.2020.108704>.
- [84] D.Y. Kovalev, M.A. Luginina, S.G. Vadchenko, X-ray diffraction study of self-propagating high-temperature synthesis in the Zr–Al–C system, *Russ. J. Inorg. Chem.* 62 (2017) 1638–1644, <https://doi.org/10.1134/S0036023617120117>.
- [85] S. Gupta, E.N. Hoffman, M.W. Barsoum, Synthesis and oxidation of Ti2InC, Zr2InC, (Ti0.5,Zr0.5)2InC and (Ti0.5,Hf0.5)2InC in air, *J. Alloys Compd.* 426 (2006) 168–175, <https://doi.org/10.1016/j.jallcom.2006.02.049>.
- [86] A.S. Farle, C. Kwakernaak, S. van der Zwaag, W.G. Sloof, A conceptual study into the potential of Mn+1AXn-phase ceramics for self-healing of crack damage, *J. Eur. Ceram. Soc.* 35 (2015) 37–45, <https://doi.org/10.30684/etj.33.4A.8>.
- [87] S.G. Vadchenko, D.Y. Kovalev, M.A. Luginina, Ignition and phase formation in the Zr–Al–C system, *Combust. Explos. Shock Waves* 53 (2017) 171–175, <https://doi.org/10.1134/S0010508217020071>.